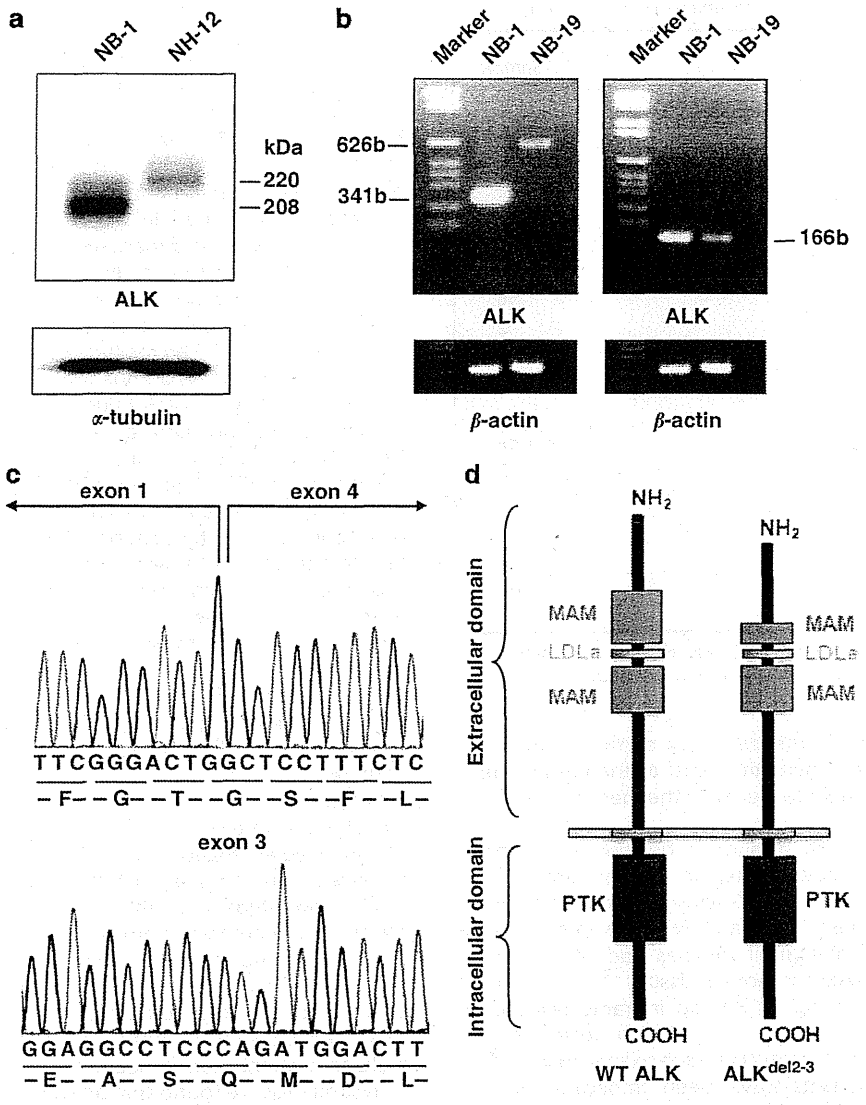

Figure 1. Detection of an aberrant truncated form of ALK in NB-1 cells. (**a**) Western blot analysis of ALK in neuroblastoma-derived cell lines. NB-1 cells strongly expressed the truncated form with a molecular mass of 208 kDa. In contrast, wild-type ALK-expressing neuroblastoma-derived cell lines (NH-12) revealed an ALK protein with a molecular mass of 220 kDa. α-Tubulin staining as loading control. (**b**) RT-PCR analysis of *ALK* exons 1-5 and exons 2 and 3 in the neuroblastoma cell lines. A short PCR product with 314 bp was detected in NB-1 cells, whereas much longer PCR products with 627 bp were detected in NB-19 cells with wild-type *ALK*. Wild-type *ALK* was detected in both NB-1 and NB-19 cells using *ALK* exon 2 and 3 primers. (**c**) Subsequent sequence analysis of *ALK* cDNA from NB-1. In-frame deletion in exons 2 and 3 was confirmed by direct sequencing. Sequencing of the PCR product detected by RT-PCR for *ALK* exons 2 and 3 confirmed the presence of wild-type *ALK* in NB-1 cells. Lower panel represents DNA sequencing for *ALK* exon 3 in NB-1 cells. (**d**) Schematic representation of the truncated form of aberrant ALK. The extracellular domain of ALK comprises two MAM domains (aa 264-427 and 480-626), one low-density lipoprotein class A (LDLa) motif (aa 453-471) and a glycine-rich region (aa 816-940) (Palmer *et al.*[30]). Because exons 2 and 3 of *ALK* implicate 224-318 aa, the in-frame deleted mutant led to a translational truncated form of the first MAM domain. PTK, protein tyrosine kinase.

siRNA, but the suppression apparently decreased in wild-type ALK-expressing NH-12 cells (Figures 6b and c). As shown in Supplementary Figure S3, significant inhibition was observed in NB-1 cells with ALK knockdown compared with that in the negative control ($P<0.05$, Mann-Whitney *U*-test).

DISCUSSION

Deregulated activation of ALK has been implicated in various human cancers through either generation of fusion proteins, overexpression or single amino-acid changes. In this study, we described a novel mechanism of oncogenic activation of *ALK* that operated in a neuroblastoma-derived cell line, NB-1. In NB-1 cells, an aberrant form of *ALK* that lacks exons 2 and 3 was amplified, leading to high-level expression of an N-terminal-truncated kinase, ALK^{del2-3}, and our functional studies confirmed the oncogenic role of ALK^{del2-3}. First, ALK^{del2-3} underwent autophosphorylation in NB-1 and NIH3T3 cells and demonstrated enhanced kinase activity, promoting downstream signaling pathways such as the STAT3 pathway. Second, ALK^{del2-3} promoted colony formation in soft agar and tumorigenicity when transduced into NIH3T3 cells in nude mice. Finally, inhibition of cell growth was observed when we treated NB-1 cells with TAE684, an ALK-specific kinase inhibitor, and siRNA-mediated gene knockdown. Unfortunately, screening of 71 primary neuroblastoma specimens and 23 neuroblastoma-derived cell lines did not identify a similar mechanism of ALK oncogenic activation in neuroblastoma; therefore, it is not a common mechanism for ALK activation in

Table 2. Neuroblastoma fresh tumor samples used in this study

Clinicopathological findings	*Samples*
Age (years)	
>1	41
<1	30
Stage	
1	16
2	11
3	12
4	29
4S	2
ND	1
MYCN status	
Amplification (+)	11
(−)	58
ND	2
ALK status	
Amplification	1
Mutation	6
Wild type	64
Total	71

Abbreviations: ALK, anaplastic lymphoma kinase; ND, not determined.

neuroblastoma. Nevertheless, the discovery of this unique ALK form will add to our knowledge with regard to the pathogenesis of neuroblastoma and will help to elucidate the mechanism of ALK activation.

Abnormal activation of RTK through a deletion in its extracellular domain has been documented in several cancers.[19-21] A common example of abnormal RTK activation is the epidermal growth factor receptor class III variant, which is present in a substantial proportion of malignant gliomas and other human cancers, but completely absent in normal tissues.[22,23] This variant results from a transcript having an 801-bp in-frame deletion of EGFR that corresponds to exons 2–7, which leads to the generation of a protein with a truncated extracellular domain.[21,24] Several molecular mechanisms have been implicated in the oncogenic pathway with epidermal growth factor receptor class III variant downstream signaling.[21,24] For example, in addition to ligand-independent self-dimerization, epidermal growth factor receptor class III variant has been shown to constitutively interact with adaptor proteins SHC and GRB2, which are involved in the recruitment of the RAS pathway.[25] The recepteur d'origine nantais (RON) RTK variant with a deletion in the first immunoglobulin-plexin transcription domain (RONΔ160) has also been considered as a constitutively activated kinase in several human cancers.[20,26] RON belongs to the MET proto-oncogene family, which plays a critical role in epithelial cell homeostasis and tumorigenic development.[27] RONΔ160 is derived from a *RON* mRNA transcript by alternative splicing that eliminates 109 aa residues from the extracellular domain of RON β-chain and is expressed in >50% of primary colon cancers and 90% of brain tumors, but not in any normal tissues.[26,28] The deleted 109 aa residues are encoded by exons 5/6, which constitute the first immunoglobulin-plexin transcription domain in the RON β-chain.[26,28] The mechanism for the oncogenic activation of RONΔ160 is believed to be one in which the deletion in the extracellular domain causes conformational changes in the kinase and leads to spontaneous dimerization, which in turn causes constitutive receptor phosphorylation and increased intracellular signaling activation.[26,28,29]

The $ALK^{del2\text{-}3}$ variant consists of a 282-bp in-frame deletion of *ALK* that corresponds to 224–318 aa in the first MAM domain (Figure 1d). ALK is the sole RTK that contains MAM domains in its extracellular region.[30] Although MAM domains are thought to participate in cell–cell interactions, their significance in ALK function remains unclear.[15,16] Thus, the functional significance of MAM deletion in the truncated ALK is still elusive. As the deleted region of *ALK* detected in NB-1 cells is in close proximity to a ligand-binding domain (391–401 aa), this deletion may structurally alter the ligand-binding domain. Similar to epidermal growth factor receptor class III variant and RONΔ160, the $ALK^{del2\text{-}3}$ variant may be constitutively activated in a ligand-independent manner and/or through spontaneous dimerization, although the exact mechanism of constitutive activation of $ALK^{del2\text{-}3}$ is yet to be elucidated.

Oncogenic ALK transformation is mediated by interactions with downstream molecules that trigger a substantial intercellular signaling cascade.[31] The most relevant and best-characterized ALK downstream pathways are the RAS-ERK, JAK3-STAT3 and PI3K-AKT pathways.[31] Among ALK signaling molecules, STAT3 is only strongly phosphorylated by $ALK^{del2\text{-}3}$, suggesting that besides F1174L or K1062M ALK mutants,[7] $ALK^{del2\text{-}3}$ would be exclusively involved in the STAT3 pathway. Recently, it has been reported that the oncogenic mutant of fms-like tyrosine kinase-internal tandem duplication aberrantly activates STAT5 when localized at ER, but fails to activate MAPK and AKT signaling.[17] Thus, this raises the possibility that involvement of the STAT3 pathway in $ALK^{del2\text{-}3}$-expressing cells resembles the fms-like tyrosine kinase-internal tandem duplication mutant.[17] Immunofluorescence staining and the endoglycosidase-H sensitivity assay revealed that $ALK^{del2\text{-}3}$ is mainly located at ER and aberrantly activates the STAT3 pathway from ER. Taken together, our results suggest that intracellular activation of $ALK^{del2\text{-}3}$ switches downstream signaling to the ALK pathway.[18]

Furthermore, ERK phosphorylation was similarly elevated in cells expressing wild-type or F1174L ALK. This may have been because of enhanced expression of exogenous wild-type *ALK* by retrovirus-mediated gene transfer. Schulte *et al.*[32] reported that the high level of wild-type ALK and mutant ALK expression has similar effects on the neuroblastoma biological phenotype, which may be related to tumor growth. Taken together, the results from our study and from the study by Schulte *et al.*[32] suggest that in addition to the ALK mutants, elevated wild-type ALK expression also mediates similar molecular functions that contribute to the malignant phenotype in neuroblastoma.

In summary, we found that an N-terminal-truncated ALK protein observed in a neuroblastoma-derived cell line (NB-1) is a novel oncogenic isoform of ALK. This study provides a better understanding of the molecular mechanism of pathogenesis of neuroblastoma as well as oncogenic roles of ALK pathway.

MATERIALS AND METHODS

Specimens

In all, 24 neuroblastoma cell lines were used in this study (Table 1). The SCMC-N series was established in our laboratory.[33] The SJNB series and UTP-N-1 cells were provided by Dr AT Look and Dr A Inoue, respectively. Other cell lines were obtained from the Japanese Cancer Resource Cell Bank (http://cellbank.nibio.go.jp/wwwjcrbj.htm). All cells were maintained in RPMI 1640 medium (Gibco, Grand Island, NY, USA) supplemented with 10% fetal bovine serum in a humidified atmosphere containing 5% CO_2 at 37 °C. Primary neuroblastoma specimens were obtained through surgery or biopsy from patients who were diagnosed with neuroblastoma and who were admitted to Tokyo University Hospital, Saitama Children's Medical Center or various other hospitals between November 1993 and October 2006. The patients were staged according to the International Neuroblastoma Staging System,[34] and the clinicopathological findings are listed in Table 2.

ALK expression analyses

Total cellular proteins were resolved on a 5–10% gradient sodium dodecyl sulfate-polyacrylamide gel and electrophoretically transferred onto

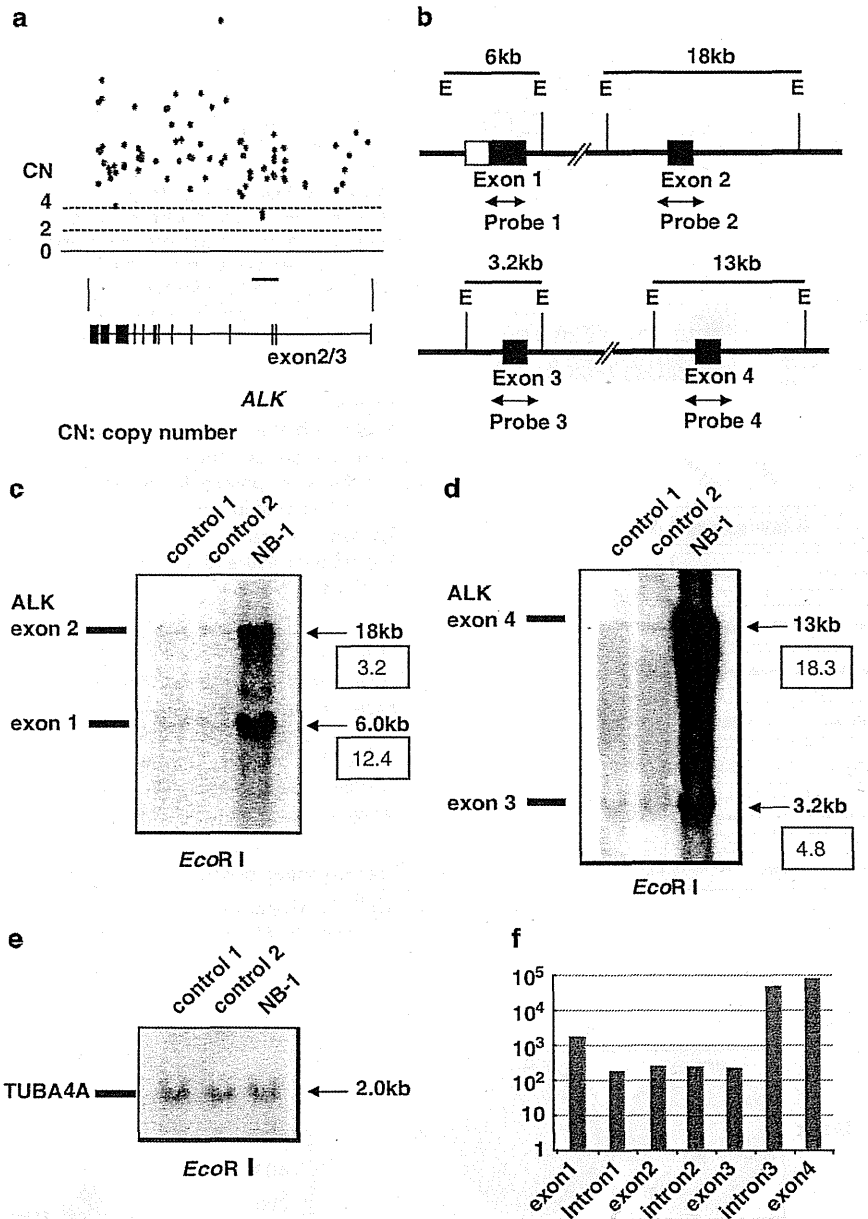

Figure 2. Genetic characteristics of the N-terminal-truncated form of ALK. (**a**) High-grade amplification of the *ALK* locus detected in NB-1 cells by single-nucleotide polymorphism array analysis (Affymetrix GeneChip 250k *Nsp*I). Among the single-nucleotide polymorphism probes located within the *ALK* amplicon, three consecutive single-nucleotide polymorphism probes (Chr2: 29 911 541 and 29 912 210) located within *ALK* intron 3 showed relatively low signal intensities. The red line indicates the focal deletion within *ALK* intron 3. (**b**) Physical maps of *ALK* exons 1–4. The restriction sites and probe maps for *ALK* exons 1–4 are indicated. E: *Eco*R1. Arrows indicate probe positions. (**c**, **d**) Southern blot analysis using *ALK* exon 1–4 probes (**c**: exons 1 and 2; **d**: exons 3 and 4). Normal peripheral blood DNA was used as a germline control. Densitometric analysis was performed using the ImageQuant 400 and ImageQuant TL software version 7. (**e**) The TUBA4A probe was used as a loading control. (**f**) Quantitative genomic PCR analysis of *ALK* using seven primer sets located within *ALK* exons 1–4. The signal intensities of *ALK* introns 1 and 2 and exons 2 and 3 were lower compared with those of *ALK* exons 1 and 4 in NB-1 cells.

polyvinylidene difluoride membranes. After blocking with 5% milk in Tris-buffered saline containing 0.1% Tween (10 mM Tris-HCl (pH 7.4), 150 mM NaCl and 0.1% Tween-20), membranes were incubated for 1 h with primary antibody in TBS-T, washed and incubated for 12 h with primary antibody in 3% bovine serum albumin. The membranes were then washed again and incubated with anti-rabbit immunoglobulin G at room temperature for 1 h. Subsequently, they were extensively washed, and the proteins were visualized by enhanced chemiluminescence (Millipore, Bedford, MA, USA). Total RNA was extracted from the 24 cell lines and 71 frozen stocked tumors using Isogen reagent (Nippon Gene, Osaka, Japan) according to the manufacturer's instructions; the total RNA was analyzed by RT-PCR to synthesize cDNA using the SuperScript Preamplification System for first-strand cDNA synthesis (Life Technologies Inc., Rockville, MD, USA). RT-PCR analysis for *ALK* expression was performed as described previously,[7] using the primer sets listed in Table 3. cDNA concentration was equalized using *β-actin* expression as a control.

Southern blot analysis

High-molecular-weight DNA was prepared from cells according to standard procedures using the QIAamp DNA Mini kit (Qiagen, Valencia, CA, USA) and a modification of the protocol provided by the manufacturer.

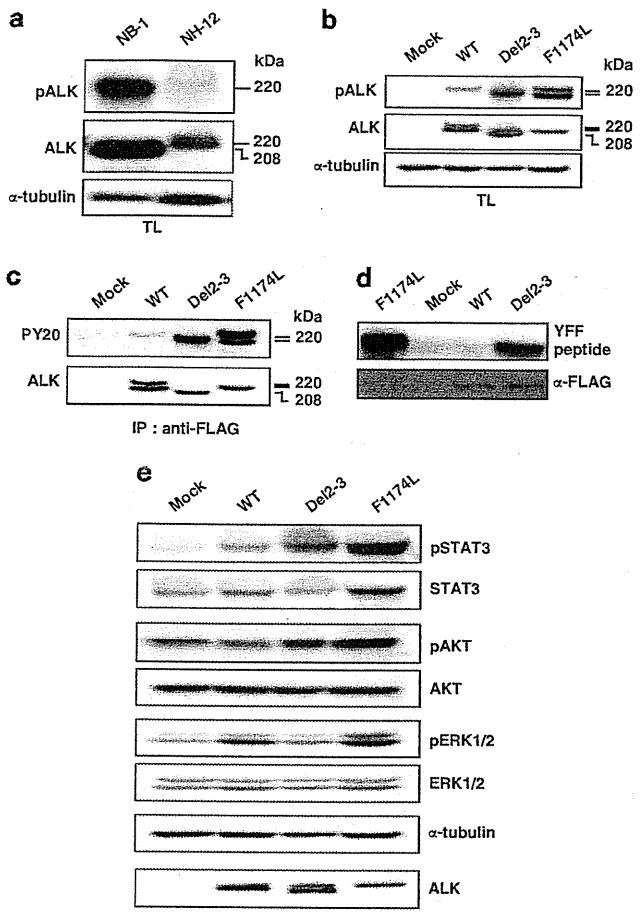

Figure 3. Kinase activities of ALK mutants and their downstream status. (**a**) Western blot analysis of ALK and phosphorylated ALK in NB-1 and NH-12 cells. NB-1 cells strongly expressed the truncated form of ALK and phosphorylated ALK compared with that in NH-12 cells. TL: Total cell lysates. (**b**) Western blot analysis of NIH3T3 cells stably expressing ALK mutants (ALK^{del2-3} and ALK^{F1174L}) and wild-type ALK. (**c**) Stably expressed ALK mutants and wild-type ALK were immunoprecipitated with an anti-FLAG antibody and subjected to western blot analysis with anti-PY20. (**d**) *In vitro* kinase assay for wild-type ALK and its mutants using the synthetic YFF peptide as a substrate. (**e**) Western blot analysis of NIH3T3 cells stably expressing ALK mutants and wild-type ALK for their downstream effectors, STAT3 (pSTAT3), AKT (pAKT) and ERK (pERK). The total amount of each molecule is also shown together with an α-tubulin blot.

DNA was extracted from NB-1 cells and peripheral normal blood cells. For Southern blot analysis, 10 μg genomic DNA was restricted with *Eco*RI and loaded onto an agarose gel.[35] After electrophoresis, the DNA was transferred to polyvinylidene difluoride membranes and hybridized with radiolabeled probes for *ALK* exons 1–4 listed in Table 3. The signal intensity of each band was quantified and calculated using the ImageQuant 400 and ImageQuant TL software version 7 (GE Healthcare, Piscataway, NJ, USA).

Quantitative genomic PCR analysis

Quantitative genomic real-time PCR was performed using SYBR Green-based quantification (Bio-Rad Laboratories, Hercules, CA, USA). The standard curve method was used to calculate the target genome numbers in the NB-1 cell line. The relative target copy number was normalized to normal human genomic DNA as a calibrator. The primer sequences used for quantitative genomic PCR are shown in Table 3.

Transforming potential of ALK mutants

ALK^{WT}-FLAG and ALK^{F1174L}-FLAG were FLAG-tagged cDNAs for wild-type *ALK* and its F1174L mutant, respectively. FLAG-tagged cDNA for the

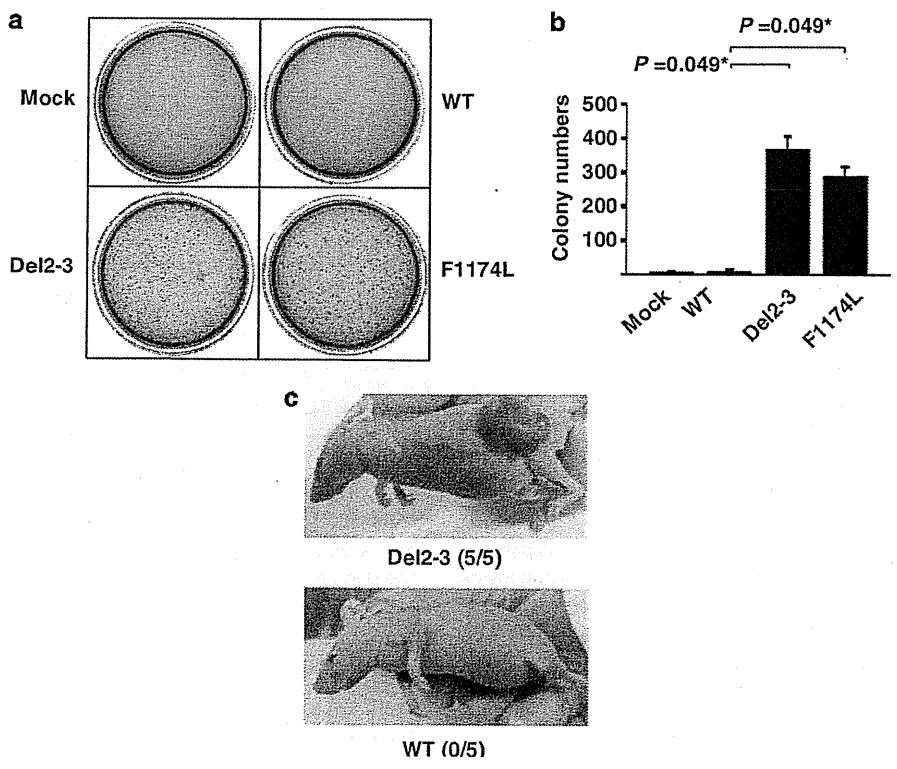

deletion mutant ($ALK^{del2\text{-}3}$-FLAG) was isolated from total RNA of NB-1 cells by high-fidelity PCR. After re-sequencing, each cDNA was constructed into the pcDNA3 expression plasmid and transfected into NIH3T3 cells using Effectene Transfection Reagents (Qiagen, Tokyo, Japan). Kinase assays were performed with stable clones in these constructs. For western blot analysis of mutant ALK and colony formation assays, NIH3T3 cells were stably transduced with wild-type and mutant ALK by retrovirus-mediated gene transfer. FLAG-tagged cDNA for wild-type and mutated ALK were then

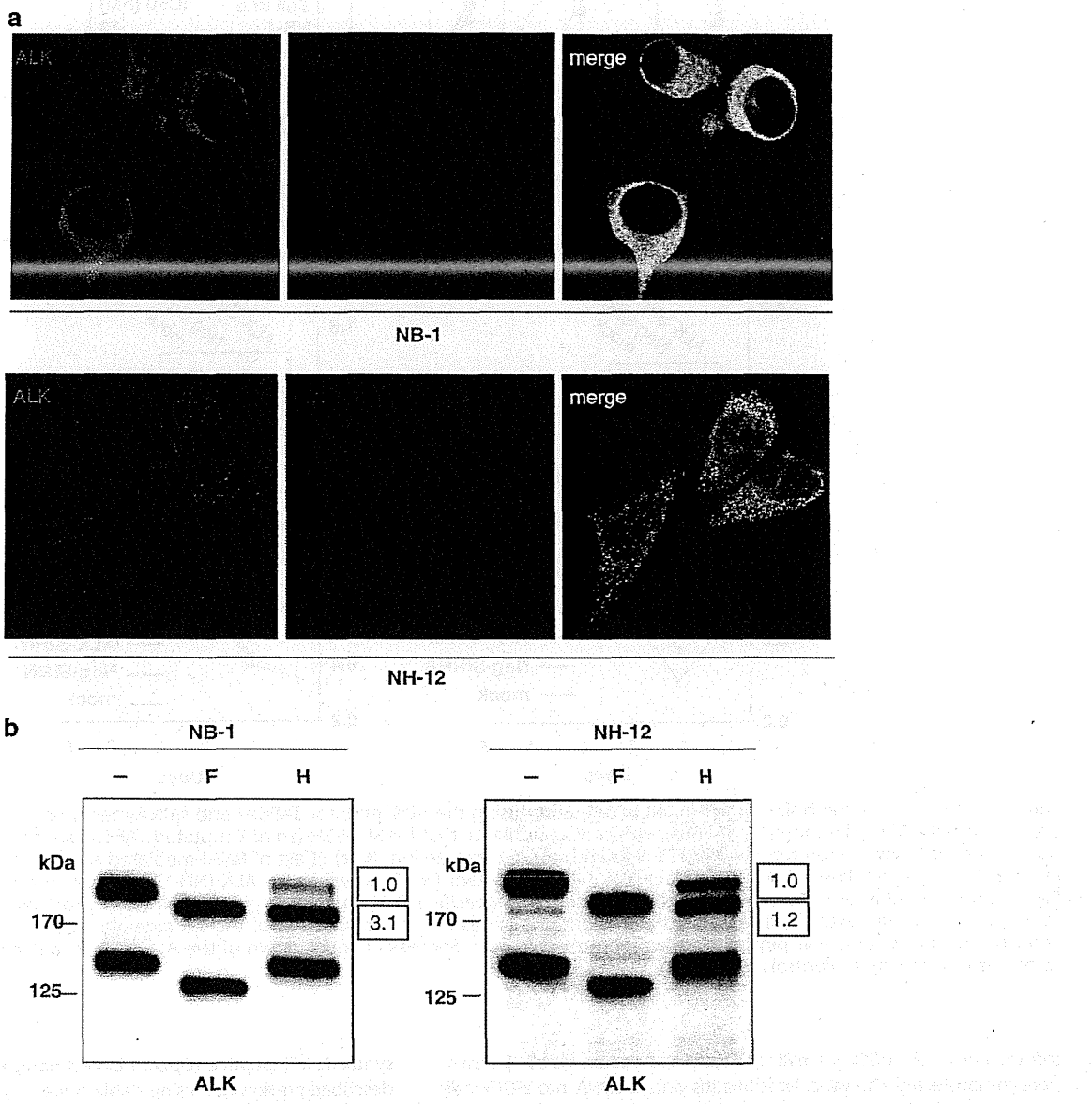

Figure 5. ER retention in the NB-1 neuroblastoma cell line and glycoprotein maturation. (**a**) Immunofluorescence confocal microscopy analysis of ALK ER localization in the neuroblastoma cell lines. The NB-1 and NH12 neuroblastoma cell lines were immunostained with the indicated antibodies and imaged using immunofluorescence microscopy to demonstrate ALK and PDI (ER-specific marker) colocalization. Cells were immunostained for ALK (red) and PDI (green), respectively. (**b**) The band of $ALK^{del2\text{-}3}$ protein of NB-1 cells is endoglycosidase H sensitive. Cell lysates from the NB-1 and NH12 neuroblastoma cell lines were incubated with N-glycosidase F (lane 2, F) and endoglycosidase H (lane 3, H). Deglycosidation profiles were compared with untreated cell lysates (lane 1). Digestion products were analyzed by western blot analysis using monoclonal anti-ALK. Signal intensities of bands in the lane endoglycosidase H were quantified by densitometric scanning using the ImageQuant 400 and ImageQuant TL software version 7. Signal intensity of approximate190 kDa band that revealed sensitivity to endoglycosidase H in NB-1 cells showed 3.1-fold higher than that of upper band.

Figure 4. Oncogenic role of the aberrant truncated form of ALK. (**a**) NIH3T3 cells stably expressing mutant kinases ($ALK^{del2\text{-}3}$ and ALK^{F1174L}) showed increased colony formation in soft agar compared with cells expressing wild-type kinase. (**b**) The average numbers of colonies in triplicate experiments are plotted. Standard deviation is indicated. Results showing significant differences compared with experiments using wild-type ALK are indicated by asterisks with *P*-values. (**c**) *In vivo* tumorigenicity assay in nude mice. Tumor formation assay in nude mice in which 1.0×10^7 NIH3T3 cells expressed wild-type ALK and the $ALK^{del2\text{-}3}$ mutant by the calcium phosphate method. Tumor formation was evaluated 21 days after inoculation.

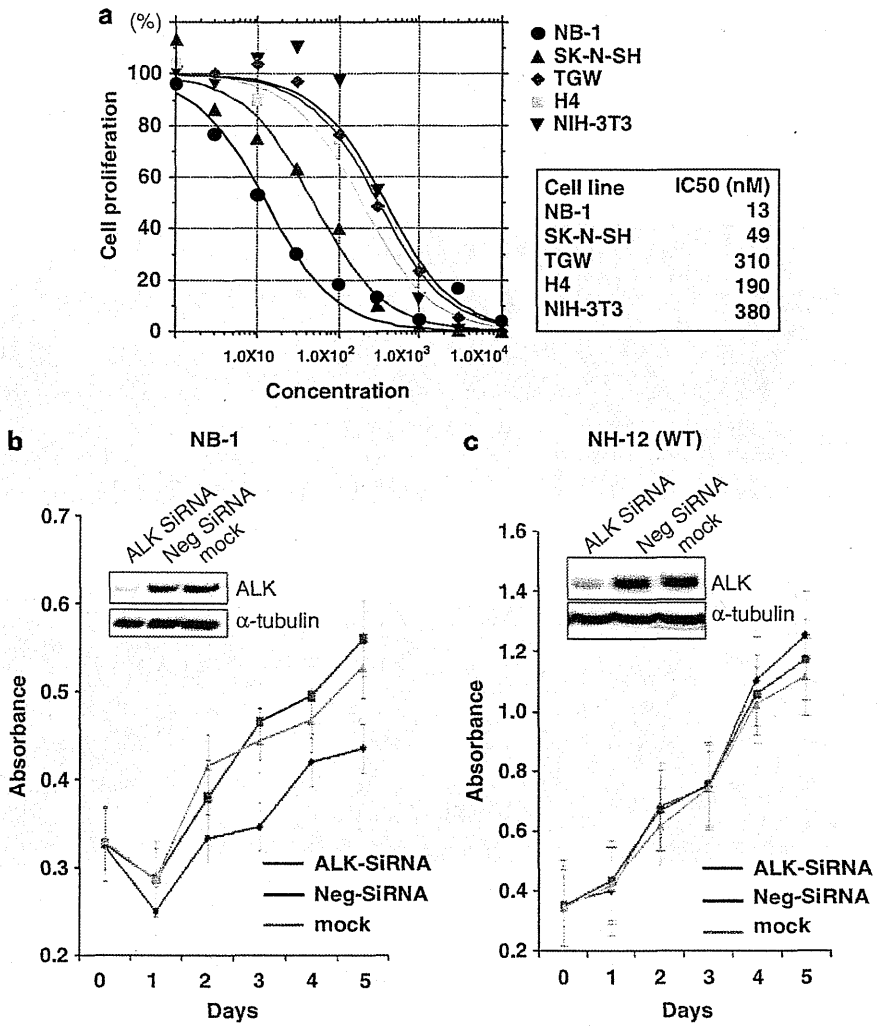

Figure 6. Effect of ALK inhibition on NB-1 cell proliferation using the ALK inhibitor TAE684 and siRNA-mediated ALK knockdown. (**a**) NB-1 cell growth was effectively inhibited by TAE684, with an IC_{50} similar to that for SK-N-SH (an *ALK*-mutated TAE684-sensitive neuroblastoma cell line), but substantially lower than that for NIH3T3 cells with no ALK expression. (**b**, **c**) Effect of RNAi-mediated ALK knockdown on cell proliferation in neuroblastoma cell lines expressing either the $ALK^{del2\text{-}3}$ mutant (NB-1) or wild-type ALK (NH-12). Cell growth was measured using the Cell Counting kit-8 after knockdown experiments using ALK-specific siRNAs, negative control siRNAs or mock experiments, in which absorbance was measured in triplicate and averaged for each assay. The mean ± s.d. of the average absorbance in three independent knockdown experiments was plotted to draw the growth curves. Successful knock down of the ALK protein was confirmed by anti-ALK blots using α-tubulin blots as controls.

constructed in the pGCDNsamIRESKO retrovirus vector. Vector plasmids were co-transfected with vesicular stomatitis virus-G cDNA into 293GP cells to obtain a retrovirus-containing supernatant, which was then transduced into 293GPG cells to stable cell lines capable of producing vesicular stomatitis virus-G-pseudotyped retroviral particles on induction.

Functional analyses of a short-form ALK

To evaluate the phosphorylation status of the ALK mutants, stable clone cell lysates were subjected to western blot analysis with anti-ALK and the antibody-specific pTyr1604 (Cell Signaling Technology, Danvers, MA, USA) of ALK. Immunoprecipitation with antibodies to FLAG (Sigma, St Louis, MO, USA) were subjected to western blot analysis with a generic antiphosphotyrosine antibody (PY20). Western blot analyses were also performed using anti-ERK1/2, anti-phospho-ERK1/2, anti-AKT, anti-phospho-AKT, anti-STAT3 and anti-phospho-STAT3 antibodies (Cell Signaling Technology). AKT and STAT3 phosphorylation signals were quantitated by densitometric scanning using the ImageQuant 400 and ImageQuant TL software version 7 (GE Healthcare). The *in vitro* kinase assay was performed with the synthetic YFF peptide (Operon Biotechnologies, Reutlingen, Germany), as described previously,[36] using stable clones in pcDNA vector constructs. We also used the *in vitro* kinase assay for wild-type and mutant *ALK* expression in NIH3T3 cells by retrovirus-mediated gene transfer using the poly-GluTyr peptide. Cell extracts were immunoprecipitated with anti-Flag antibody, and the expression was subjected to immunoblotting using anti-ALK antibody. ALK mutant kinase activity was measured using a non-radioactive isotope solid-phase enzyme-linked immunosorbent assay in the Universal Tyrosine Kinase Assay kit (Takara Bio, Osaka, Japan). Assays were performed in 40 mM Tris (pH 7.4), 20 mM $MgCl_2$, 2 mM dithiothreitol and 0.1 mg/ml bovine serum albumin buffer.

Transforming potential of short-form ALK

For colony assays, 1×10^3 stably transfected NIH3T3 cells were mixed in 0.4% agarose with 10% fetal bovine serum–Dulbecco's modified Eagle's medium and plated on 0.6% agarose-coated 35-mm dishes. After culturing for 14 days, colonies measuring 0.1 mm in diameter were counted. Colonies were quantified during triplicate experiments. Tumor formation

Table 3. Primer sets used in this study

	Primer sequence (5′→3′)		*Annealing temperature (°C)*
	Forward	*Reverse*	
RT-PCR analyses			
ALK exon 1/5	CTTCTCTTCCAGATCTTCGG	ATTCAGGGCAAAGAAGTCCAC	55
Exon 1/2	AAGCAGTTGGTGCTGGAGCT	TTTGACTTCCCCTGTGAGCT	55
Exon 2/4	CATAGCTCCTTGGAATCACC	ATGAGGAGCAGCAGTGAGCA	55
Exon 4/5-6	TTCTCAACACCTCAGCTGAC	ACTGCAGTGAAGGAACATCC	55
Exon 5/8-9	GAAACCGCAGCTTGTCTGCA	CGATCAAGAGCTCTCCATGT	55
Exon 8/12	AAGTGCTACAGTGACCAGTG	TAGCGGAGAGGACAAGATC	55
Exon 11/14	ATATCTCCATCAGCCTGGAC	AAGAACACCATGATGCGGTC	55
Exon 13/15-16	CCTGAAAGGCATCCAGATCT	AAGATGAAGGATGGAGTGCC	55
Exon 15/17	AATCCGTGTGAACAGAAGCG	TGGAGGAGGCGGAGGATATA	55
Exon 17/19-20	AAATCTTTGCAGGAGGGTGC	GCGTCTCCTGCATTGTGTCA	55
Exon 20/23	TTTCTCCGGCATCATGATTG	CTCATGGAAGCCCTGATCAT	55
Exon 23/26	TGCCTGAAGTGTGCTCTGAA	GATTGGAGACTTCGGGATGG	55
Exon 26/30	AGAAACTGCCTCTTGACCTG	GGACCCGGATGTAATCAACA	55
Exon 29/30	GGAGAGGATTGAATACTGCA	GTTGCACAAGGTCCACGGAT	55
Exon 30/30	TGCAGAGATCTCTGTTCGAG	GTTGCACAAGGTCCACGGAT	55
Exon 30/30	TAACGTTGCAACTGGGAGAC	GTTGCACAAGGTCCACGGAT	55
β-Actin	CTTCTACAATGAGCTGCGTG	TCATGAGGTAGTCAGTCAGC	55
Southern blot analyses			
ALK exon 1	AGAGTCTGGCAGTTGACTTC	TGCTCACAAACAGTCCCGAAG	60
Exon 2	TCAACTCAGTCTACTGGTGG	GGATATGGCAGACACAAAGC	60
Exon 3	AGCCCTGTGGTATTGACAAC	AGATGGGACTTGTCTTCCTC	60
Exon 4	AGAATGGAGGAAGAAGGCTG	GTAATTGCTCAACCTGGACC	60
TUBA4A	CTCTCACACTCTGGTATCTC	CTGACCATTAGCACAGTCTC	60
Quantitative genomic PCR analyses			
ALK exon 1	CTCAGCGAGCTGTTCAGTTG	CAGTCCCGAAGATCTGGAAG	55
Intron 1	CTGCTTGGTTCCTCACATCC	GTCTGAGTCATTGGCTAATCTCA	55
Exon 2	ACCCAAGCACATGGATCAG	GATGAGACAGGAAAGGGAAGG	55
Intron 2	GGTATACACGTGCCATGGTG	CCAAATACGGCATGTTCTCA	55
Exon 3	GGAGTGCAGCTTTGACTTCC	CTGGGCATCTCCTTAGAACG	55
Intron 3	TGGCATGATTGATTACCCAAG	CTGGAGATCACCCTTTGAGG	55
Exon 4	CAACACCTCAGCTGACTCCA	CTCTCTTGCAGCCTCGTTG	55

Abbreviations: ALK, anaplastic lymphoma kinase; RT-PCR, reverse transcription-polymerase chain reaction.

assay was performed in nude mice, in which 1.0×10^7 NIH3T3 cells expressing wild-type *ALK* and $ALK^{del2\text{-}3}$ mutant were injected by the calcium phosphate method. Tumor formation was evaluated 21 days after inoculation as described previously.[6]

Immunofluorescence

Cells were fixed for 10 min with 4% paraformaldehyde and washed three times with phosphate-buffered saline. After 1 h of blocking in phosphate-buffered saline containing 4% donkey serum and 0.1% Triton X-100/phosphate-buffered saline, the cells were incubated for 2 h in the same buffer with polyclonal anti-ALK (Santa Cruz Biotechnology, Santa Cruz, CA, USA) and monoclonal anti-PDI (Abcam, Cambridge, MA, USA), respectively. The cells were then washed three times with phosphate-buffered saline before and after incubation with anti-mouse IgG Alexa Fluor 488 and anti-rabbit IgG Alexa Fluor 594-conjugated secondary antibodies, respectively, (Invitrogen, Carlsbad, CA, USA). The cells were then mounted in Prolong Gold (Invitrogen). Confocal laser microscopy was performed using a Fluoview 10 000 confocal microscope (Olympus, Tokyo, Japan). Colocalization of ALK and PDI was quantified using the Pearson's correlation coefficient and determined through correlation analysis with a Fluoview 1000 software.[37]

Deglycosylation of ALK with N-glycosidase F, N-glycosidase H and O-glycosidase

Proteins from cell lysates obtained from neuroblastoma cell lines NB-1 and NH-12 were incubated with N-glycosidase F and endoglycosidase H for deglycosylation (New England Biolabs, Ipswich, MA, USA), following the manufacturer's instructions.[18] The samples were then used for immunoblotting with anti-ALK antibody. Signal intensities of bands in the lane endoglycosidase H were quantified by densitometric scanning using the ImageQuant 400 and ImageQuant TL software version 7.

ALK inhibition by an ALK inhibitor and siRNA-mediated knockdown in neuroblastoma cells

A partial *ALK*-deleted neuroblastoma-derived cell line (NB-1), *ALK*-mutated neuroblastoma-derived cell lines (SK-N-SH and TGW) and a glioblastoma-derived cell line (H4) were cultured with varying concentrations of the ALK inhibitor TAE684,[8] and cell growth was measured using the CellTiter-Glo Luminescent Cell Viability Assay (Promega, Tokyo, Japan). NIH3T3 cells were used as a control. The IC_{50} value of TAE684 against NB-1 cells was calculated by nonlinear regression (variable slope) using the GraphPad Prism 5 software (GraphPad, La Jolla, CA, USA). NB-1 and NH-12 cells with wild-type ALK were transfected with either an *ALK*-specific siRNA or a nonspecific siRNA, as described previously.[7] To assess the effect of ALK knockdown on cell growth, cells were seeded in 96-well plates at a concentration of 1.0×10^4 cells per well 24 h before transfection and assayed using the Cell Counting kit-8 (Dojindo, Kumamoto, Japan). We also performed an siRNA-mediated ALK knockdown cell proliferation assay using a cell counter and 6-well plates. These cells were seeded in 6-well plates at a concentration of 2.0×10^5 cells per well 24 h before transfection. The number of cells was counted after 72 h using cytorecon (ECI, Tokyo, Japan).

Statistical analyses

The Mann-Whitney *U*-test was used to compare the differences in colony formation as well as the effects of ALK knockdown on cell growth between wild-type and ALK mutants. Phosphorylation signals of downstream molecules were evaluated by Student's *t*-test.

CONFLICT OF INTEREST

The authors declare no conflict of interest.

ACKNOWLEDGEMENTS

We thank Mrs Matsumura, Mrs Hoshino, Mrs Yin, Miss Ogino and Mrs Saito for their excellent technical assistance. We would also thank Dr Tanaka, Dr Saito, Mr Shiosaka and Mrs Mori for useful advice concerning biological analysis; Dr AT Look, Harvard Medical University, and Dr A Inoue, St Jude Children's Research Hospital, for their generous gifts of neuroblastoma cell lines. This work was supported by Research on Measures for Intractable Diseases, Health and Labor Sciences Research Grants, Ministry of Health, Labor and Welfare, Research on Health Sciences focusing on Drug Innovation, the Japan Health Sciences Foundation and Core Research for Evolutional Science and Technology, Japan Science and Technology Agency.

REFERENCES

1 Morris SW, Kirstein MN, Valentine MB, Dittmer K, Shapiro DN, Look AT *et al.* Fusion of a kinase gene, ALK, to a nucleolar protein gene, NPM, in non-Hodgkins-lymphoma (Vol 263, PG 1281, 1994). *Science* 1995; **267**: 316-317.
2 Shiota M, Nakamura S, Ichinohasama R, Abe M, Akagi T, Takeshita M *et al.* Anaplastic large-cell lymphomas expressing the novel chimeric protein P80(NPM/ALK)–a distinct clinicopathological entity. *Blood* 1995; **86**: 1954-1960.
3 Griffin CA, Hawkins AL, Dvorak C, Henkle C, Ellingham T, Perlman EJ. Recurrent involvement of 2p23 in inflammatory myofibroblastic tumors. *Cancer Res* 1999; **59**: 2776-2780.
4 Jazii FR, Najafi Z, Malekzadeh R, Conrads TP, Ziaee AA, Abnet C *et al.* Identification of squamous cell carcinoma associated proteins by proteomics and loss of beta tropomyosin expression in esophageal cancer. *World J Gastroenterol* 2006; **12**: 7104-7112.
5 Rikova K, Guo A, Zeng Q, Possemato A, Yu J, Haack H *et al.* Global survey of phosphotyrosine signaling identifies oncogenic kinases in lung cancer. *Cell* 2007; **131**: 1190-1203.
6 Soda M, Choi YL, Enomoto M, Takada S, Yamashita Y, Ishikawa S *et al.* Identification of the transforming EML4-ALK fusion gene in non-small-cell lung cancer. *Nature* 2007; **448**: 561-5U3.
7 Chen YY, Takita J, Choi YL, Kato M, Ohira M, Sanada M *et al.* Oncogenic mutations of ALK kinase in neuroblastoma. *Nature* 2008; **455**: 971-U56.
8 George RE, Sanda T, Hanna M, Frohling S, Luther W, Zhang JM *et al.* Activating mutations in ALK provide a therapeutic target in neuroblastoma. *Nature* 2008; **455**: 975-978.
9 Janoueix-Lerosey I, Lequin D, Brugieres L, Ribeiro A, de Pontual L, Combaret V *et al.* Somatic and germline activating mutations of the ALK kinase receptor in neuroblastoma. *Nature* 2008; **455**: 967-U51.
10 Mosse YP, Laudenslager M, Longo L, Cole KA, Wood A, Attiyeh EF *et al.* Identification of ALK as a major familial neuroblastoma predisposition gene. *Nature* 2008; **455**: 930-U22.
11 Maris JM, Hogarty MD, Bagatell R, Cohn SL. Neuroblastoma. *Lancet* 2007; **369**: 2106-2120.
12 De Bernardi B, Nicolas B, Boni L, Indolfi P, Carli M, di Montezemolo LC *et al.* Disseminated neuroblastoma in children older than one year at diagnosis: comparable results with three consecutive high-dose protocols adopted by the Italian Co-Operative Group for Neuroblastoma. *J Clin Oncol* 2003; **21**: 1592-1601.
13 Matthay KK, Villablanca JG, Seeger RC, Stram DO, Harris RE, Ramsay NK *et al.* Treatment of high-risk neuroblastoma with intensive chemotherapy, radiotherapy, autologous bone marrow transplantation, and 13-*cis*-retinoic acid. *N Engl J Med* 1999; **341**: 1165-1173.
14 Pearson ADJ, Pinkerton CR, Lewis IJ, Imeson J, Ellershaw C, Machin D *et al.* High-dose rapid and standard induction chemotherapy for patients aged over 1 year with stage 4 neuroblastoma: a randomised trial. *Lancet Oncol* 2008; **9**: 247-256.
15 Beckmann G, Bork P. An adhesive domain detected in functionally diverse receptors. *Trends Biochem Sci* 1993; **18**: 40-41.
16 Loren CE, Englund C, Grabbe C, Hallberg B, Hunter T, Palmer RH. A crucial role for the anaplastic lymphoma kinase receptor tyrosine kinase in gut development in *Drosophila melanogaster*. *EMBO Rep* 2003; **4**: 781-786.
17 Choudhary C, Olsen JV, Brandts C, Cox J, Reddy PNG, Boehmer FD *et al.* Mislocalized activation of oncogenic RTKs switches downstream signaling outcomes. *Mol Cell* 2009; **36**: 326-339.
18 Mazot P, Cazes A, Boutterin MC, Figueiredo A, Raynal V, Combaret V *et al.* The constitutive activity of the ALK mutated at positions F1174 or R1275 impairs receptor trafficking. *Oncogene* 2011; **30**: 2017-2025.
19 Lemmon MA, Schlessinger J. Cell signaling by receptor tyrosine kinases. *Cell* 2010; **141**: 1117-1134.
20 Lu Y, Yao HP, Wang MH. Multiple variants of the RON receptor tyrosine kinase: biochemical properties, tumorigenic activities, and potential drug targets. *Cancer Lett* 2007; **257**: 157-164.
21 Pedersen MW, Meltorn M, Damstrup L, Poulsen HS. The type III epidermal growth factor receptor mutation-biological significance and potential target for anti-cancer therapy. *Ann Oncol* 2001; **12**: 745-760.
22 Ekstrand AJ, James CD, Cavenee WK, Seliger B, Pettersson RF, Collins VP. Genes for epidermal growth-factor receptor, transforming growth factor-alpha, and epidermal growth-factor and their expression in human gliomas *in vivo*. *Cancer Res* 1991; **51**: 2164-2172.
23 Wong AJ, Ruppert JM, Bigner SH, Grzeschik CH, Humphrey PA, Bigner DS *et al.* Structural alterations of the epidermal growth-factor receptor gene in human gliomas. *Proc Natl Acad Sci USA* 1992; **89**: 2965-2969.
24 Gan HK, Kaye AH, Luwor RB. The EGFRvIII variant in glioblastoma multiforme. *J Clin Neurosci* 2009; **16**: 748-754.
25 Prigent SA, Nagane M, Lin H, Huvar I, Boss GR, Feramisco JR *et al.* Enhanced tumorigenic behavior of glioblastoma cells expressing a truncated epidermal growth factor receptor is mediated through the Ras-Shc-Grb2 pathway. *J Biol Chem* 1996; **271**: 25639-25645.
26 Zhou YQ, He C, Chen YQ, Wang D, Wang MH. Altered expression of the RON receptor tyrosine kinase in primary human colorectal adenocarcinomas: generation of different splicing RON variants and their oncogenic potential. *Oncogene* 2003; **22**: 186-197.
27 Ronsin C, Muscatelli F, Mattei MG, Breathnach R. A novel putative receptor protein tyrosine kinase of the met family. *Oncogene* 1993; **8**: 1195-1202.
28 Wang MH, Kurtz AL, Chen YQ. Identification of a novel splicing product of the RON receptor tyrosine kinase in human colorectal carcinoma cells. *Carcinogenesis* 2000; **21**: 1507-1512.
29 Chen YQ, Zhou YQ, Angeloni D, Kurtz AL, Qiang XZ, Wang MH. Overexpression and activation of the RON receptor tyrosine kinase in a panel of human colorectal carcinoma cell lines. *Exp Cell Res* 2000; **261**: 229-238.
30 Palmer RH, Vernersson E, Grabbe C, Hallberg B. Anaplastic lymphoma kinase: signalling in development and disease. *Biochem J* 2009; **420**: 345-361.
31 Chiarle R, Voena C, Ambrogio C, Piva R, Inghirami G. The anaplastic lymphoma kinase in the pathogenesis of cancer. *Nat Rev Cancer* 2008; **8**: 11-23.
32 Schulte JH, Bachmann HS, Brockmeyer B, DePreter K, Oberthur A, Ackermann S *et al.* High ALK receptor tyrosine kinase expression supersedes ALK mutation as a determining factor of an unfavorable phenotype in primary neuroblastoma. *Clin Cancer Res* 2011; **17**: 5082-5092.
33 Takita J, Yang HW, Chen YY, Hanada R, Yamamoto K, Teitz T *et al.* Allelic imbalance on chromosome 2q and alterations of the caspase 8 gene in neuroblastoma. *Oncogene* 2001; **20**: 4424-4432.
34 Brodeur GM, Pritchard J, Berthold F, Carlsen NLT, Castel V, Castleberry RP *et al.* Revisions of the international criteria for neuroblastoma diagnosis, staging, and response to treatment. *J Clin Oncol* 1993; **11**: 1466-1477.
35 Takita J, Hayashi Y, Nakajima T, Adachi J, Tanaka T, Yamaguchi N *et al.* The p16 (CDKN2A) gene is involved in the growth of neuroblastoma cells and its expression is associated with prognosis of neuroblastoma patients. *Oncogene* 1998; **17**: 3137-3143.
36 Donella-Deana A, Marin O, Cesaro L, Gunby RH, Ferrarese A, Coluccia AML *et al.* Unique substrate specificity of anaplastic lymphoma kinase (ALK): development of phosphoacceptor peptides for the assay of ALK activity. *Biochemistry* 2005; **44**: 8533-8542.
37 Smith JL, McBride CM, Nataraj PS, Bartos DC, January CT, Delisle BP. Trafficking-deficient hERG K(+) channels linked to long QT syndrome are regulated by a microtubule-dependent quality control compartment in the ER. *Am J Physiol-Cell Physiol* 2011; **301**: C75-C85.

Supplementary Information accompanies the paper on the Oncogene website (http://www.nature.com/onc)

e-Blood

Spliceosomal gene aberrations are rare, coexist with oncogenic mutations, and are unlikely to exert a driver effect in childhood MDS and JMML

Shinsuke Hirabayashi,[1] Christian Flotho,[1] Jessica Moetter,[1] Michael Heuser,[2] Henrik Hasle,[3] Bernd Gruhn,[4] Thomas Klingebiel,[5] Felicitas Thol,[2] Brigitte Schlegelberger,[6] Irith Baumann,[7] Brigitte Strahm,[1] Jan Stary,[8] Franco Locatelli,[9] Marco Zecca,[10] Eva Bergstraesser,[11] Michael Dworzak,[12] Marry M. van den Heuvel-Eibrink,[13,14] Barbara De Moerloose,[15] Seishi Ogawa,[16] Charlotte M. Niemeyer,[1] and Marcin W. Wlodarski,[1] on behalf of the European Working Group of MDS in Childhood

[1]Pediatric Hematology and Oncology, University of Freiburg, Freiburg, Germany; [2]Hematology, Hemostasis, Oncology and Stem Cell Transplantation, Hannover Medical School, Hannover, Germany; [3]Pediatrics, Aarhus University Hospital Skejby, Aarhus, Denmark; [4]Department of Pediatrics, University Hospital Jena, Jena, Germany; [5]Pediatric Hematology, Oncology and Hemostaseology, University of Frankfurt, Frankfurt, Germany; [6]Institute of Cell and Molecular Pathology, Hannover Medical School, Hannover, Germany; [7]Department of Pathology, Clinical Centre South West, Böblingen Clinics, Böblingen, Germany; [8]Pediatric Hematology and Oncology, Charles University, 2nd Faculty of Medicine and University Hospital Motol, Prague, Czech Republic; [9]Pediatric Hematology-Oncology, Istituto di Ricovero e Cura a Carattere Scientifico Ospedale Bambino Gesù, Rome, University of Pavia, Pavia, Italy; [10]Pediatric Hematology and Oncology, Fondazione Istituto di Ricovero e Cura a Carattere Scientifico Policlinico San Matteo, Pavia, Italy; [11]Hematology and Oncology, University Children's Hospital, Zurich, Switzerland; [12]St Anna Children's Hospital, Department of Pediatrics, Medical University Vienna, Vienna, Austria; [13]Department of Pediatric Oncology/Hematology, Erasmus MC, Rotterdam, The Netherlands; [14]Dutch Childhood Oncology Group, The Hague, The Netherlands; [15]Department of Pediatric Hematology-Oncology, Ghent University Hospital, Ghent, Belgium; and [16]Cancer Genomics Project, Graduate School of Medicine, University of Tokyo, Tokyo, Japan

Somatic mutations of the spliceosomal machinery occur frequently in adult patients with myelodysplastic syndrome (MDS). We resequenced *SF3B1*, *U2AF35*, and *SRSF2* in 371 children with MDS or juvenile myelomonocytic leukemia. We found missense mutations in 2 juvenile myelomonocytic leukemia cases and in 1 child with systemic mastocytosis with MDS. In 1 juvenile myelomonocytic leukemia patient, the *SRSF2* mutation that initially coexisted with an oncogenic *NRAS* mutation was absent at relapse, whereas the *NRAS* mutation persisted and a second, concomitant *NRAS* mutation later emerged. The patient with systemic mastocytosis and MDS carried both mutated *U2AF35* and *KIT* in a single clone as confirmed by clonal sequencing. In the adult MDS patients sequenced for control purposes, we detected previously reported mutations in 7/30 and a novel *SRSF2* deletion (c.284_307del) in 3 of 30 patients. These findings implicate that spliceosome mutations are rare in pediatric MDS and juvenile myelomonocytic leukemia and are unlikely to operate as driver mutations. (*Blood.* 2012;119(11):e96-e99)

Introduction

Recent whole exome sequencing studies identified recurrent somatic mutations in spliceosome complex genes in a significant proportion of adult patients with myelodysplastic syndrome (MDS).[1-3] The biologic significance of such mutations remains to be fully elucidated; some mutations (eg, those involving *SF3B1*) may correlate with a better overall survival.[2] The spectrum of spliceosome genes commonly affected includes *SF3B1* (mutated in up to 83% of refractory anemia with ringed sideroblasts), *U2AF35* (affected in up to 18% of refractory cytopenia with multilineage dysplasia), and *SRSF2* (abnormal in up to 31% of chronic myelomonocytic leukemia [CMML] cases).[1] The lesions occur as somatic heterozygous missense mutations. They cluster to 2 hotspots in *U2AF35*, targeting protein residues S34 or Q157, or to 1 hotspot in *SRSF2* (targeting P95) or *SF3B1* (targeting K700) each. The genes code for components of the splicing machinery responsible for processing of pre-mRNA to mature RNA.[1,4] We hypothesized that the disruption of the spliceosome complex might play a central role in the pathogenesis of childhood MDS and juvenile myelomonocytic leukemia (JMML). We used targeted resequencing to investigate the 4 hotspots of 3 spliceosome genes in 371 pediatric and 30 adult cases.

Methods

Patients

Pediatric patients were enrolled in study 98 or 2006 (www.clinicaltrials.gov; NCT00047268 and NCT00662090) of the European Working Group of MDS in Childhood. Adult MDS samples were enrolled in multicenter treatment trials that investigated the use of all-trans retinoic acid,[5] antithymocyte globulin (NCT00004208),[6,7] deferasirox,[8] lenalidomide, or thalidomide for treatment of MDS. Informed consent to use biologic material had been obtained from patients or patients' guardians after approval by the institutional review board of each participating institution in accordance with the Declaration of Helsinki.

Submitted December 1, 2011; accepted December 29, 2011. Prepublished online as *Blood* First Edition paper, January 11, 2012; DOI 10.1182/blood-2011-12-395087.

This article contains a data supplement.

The publication costs of this article were defrayed in part by page charge payment. Therefore, and solely to indicate this fact, this article is hereby marked "advertisement" in accordance with 18 USC section 1734.

Table 1. Study cohorts

Diagnosis, subtype at diagnosis	No.	Median age, y (range)	Female/ male	*SRSF2* P95H/L/R/del	*SF3B1* K700E	*U2AF35* (S34Y/Q157P)
Pediatric cohort, classified according to references 10-12						
Primary MDS						
RCC	123	10.5 (1.5-17.9)	54/69	0	0	1/0
RAEB/RAEB-T	56	10.4 (1.0-17.6)	24/32	0	0	0/0
MDR-AML	8	12.8 (5.8-22.4)	5/3	0	0	0/0
Secondary MDS	68	13.1 (0.6-25.4)	25/43	0	0	0/0
JMML	116	1.4 (0.1-7.0)	40/76	2	0	0/0
Adult cohort, classified according to reference 13						
CMML	5	76 (57-84)	3/2	1	0	0/0
RA	12	59 (42-73)	3/9	2	0	0/1
RCMD	5	68 (42-78)	2/3	1	1	0/0
RAEB-1/2	8	73 (68-83)	3/5	3	0	0/1

RCC indicates refractory cytopenia of childhood; RAEB, refractory anemia with excess blasts; RAEB-T, RAEB in transformation; MDR-AML, myelodysplasia-related acute myeloid leukemia; RA, refractory anemia; RCMD, refractory cytopenia with multilineage dysplasia; RAEB-1, refractory anemia with excess blasts-1; RAEB-2, refractory anemia with excess blasts-2; P95H/L/R/del, mutation of amino acid residue proline 95 to histidine/leucine/arginine/deletion; K700E, lysine 700 to glutamic acid; S34Y, serine 34 to tyrosine; and Q157P, glutamine 157 to proline.

Direct sequencing

Targeted resequencing was performed using genomic DNA as detailed in supplemental Table 1 (see the Supplemental Materials link at the top of the article). Mutations were confirmed in at least 2 independent runs.

Allele-specific clonal sequencing

TA subcloning and sequencing of bacterial colonies were performed as previously described.[9] On average, 26 colonies were sequenced per single ligated amplicon of *U2AF35* or *KIT*.

Denaturing high-performance liquid chromatography

Longitudinal denaturing high-performance liquid chromatography analysis of *NRAS* exon 1 and exon 2 was performed using primers listed in supplemental Table 1.

Results and discussion

We analyzed 4 spliceosome gene hotspots in 401 patients with MDS and JMML; the subtypes are listed in Table 1. All 371 children were enrolled in European Working Group of MDS in Childhood studies and 30 adult MDS patients participating in various clinical trials[5-8] were included. Because mutations in spliceosome genes occur somatically in leukemic cells and are not found in healthy controls (dbSNP and the 1000 Genomes databases), an additional control cohort was not included in this study. As expected, results in the adult MDS population were comparable with those reported previously[1]: 10 of 30 samples had a spliceosome mutation. The *SRSF2* gene was affected most frequently. Of 7 patients with *SRSF2* mutation, 4 carried the known mutations c.284C > T/A/G(p.P95L/H/R) and in 3 patients a novel deletion *SRSF2* c.284_307del(p.P95_R102del) was detected. The *U2AF35* and *SF3B1* mutations were discovered in 2 patients and 1 patient, respectively (Table 1).

By contrast, in the cohort of 371 children, spliceosome mutations were found in only 3 cases (Figure 1A; supplemental Figure 1). A heterozygous *SRSF2*(p.P95L) mutation, being the most prevalent mutation in adult CMML,[1] was identified in 2 JMML cases (patients SC092 and D361). Analysis of DNA from buccal epithelial cells confirmed the somatic nature of this mutation in SC092 (supplemental Figure 1). Hematopoietic cells of both children had a normal karyotype and concomitant mutations of the RAS pathway: *PTPN11*(p.E76Q) in SC092 and *NRAS*(p.G13D) in D361 (Figure 1A). Patient SC092 was successfully transplanted and is currently disease-free. Patient D361 carried a *SRSF2* and a singular *NRAS* mutation at diagnosis (Figure 1B; supplemental Figure 1D). He relapsed after hematopoietic stem cell transplantation (HSCT). At relapse, the *SRSF2*(p.P95L) mutation was no longer detectable, whereas the initial *NRAS*(p.G13D) mutation persisted. After a second HSCT, which failed to induce remission, splenectomy was performed because of acceleration of the disease. In spleen cells, the *SRSF2* mutation remained absent, but strikingly, a new *NRAS*(p.Q61K) mutation had appeared in addition to the preexisting *NRAS*(p.G13D) mutation. The hypothetical model of clonal evolution for this patient is shown in Figure 1B. At diagnosis, 2 distinct clones are postulated to exist: an *NRAS*(p.G13D)–bearing primary clone, which was outcompeted by a faster-growing but less refractory offspring clone carrying a *SRSF2*(p.P95L) mutation as an additional lesion. Although HSCT eradicated this secondary clone, the primary clone persisted and gave rise to disease recurrence. Under selective pressure exerted through second HSCT, a novel secondary clone with *NRAS* p.G13D/Q61K double mutation emerged.

The third patient with a spliceosome mutation (D717) was diagnosed at the age of 17 years with systemic mastocytosis with a *KIT*(p.D816V) mutation, normal cytogenetics, and associated clonal hematologic nonmast cell lineage disease, which resembled MDS, subtype refractory cytopenia (Figure 1C). Although the mastocytosis component of the disease responded to interferon-alpha2b, HSCT was performed for persistent thrombocytopenia and anemia. Two years after HSCT, the patient relapsed with 35% autologous cells. Allele-specific clonal sequencing of affected *U2AF35* and *KIT* exons revealed the presence of both mutations in the sample at diagnosis and at time of disease recurrence. Total allelic burdens of the 2 mutations were similar both at diagnosis and relapse (Figure 1C), indicating that the *KIT*(p.D816V) and the *U2AF35*(p.S34Y) mutations were likely present in the same clone. As previously postulated, it is probable that the systemic mastocytosis and associated clonal hematologic nonmast cell lineage disease compartments in this patient originated from a common neoplastic precursor.[14,15]

The drastically reduced frequency of spliceosome mutations in pediatric compared with adult MDS suggests a different pathogenetic mechanism in childhood disorders; the pathogenesis in children is probably more related to genetic determinants acquired prenatally and less to accumulation of somatic events during life. This view fits well with previous reports that somatic mutations of genes, such as *DNMT3A*, *TET2*, *IDH*, and *ASXL1*, are also much less prevalent in pediatric MDS.[16-19]

A

Patient	Diagnosis	Spliceosome mutation	Concomitant mutations	Age (Sex)	Karyo type	HSCT (Relapse)	Survival status
SC092	JMML	*SRSF2* c.284C>T(p.P95L)	*PTPN11* c.226G>C(p.E76Q)	4.5 years (female)	46,XX	MRD (No)	Alive 4.2 years
D361	JMML	*SRSF2* c.284C>T(p.P95L)	*NRAS* c.38G>A(p.G13D)	3.9 years (male)	46,XY	MRD (Yes)	Dead
D717	SM-AHNMD	*U2AF35* c.101C>A(p.S34Y)	*KIT* c.2447A>T(p.D816V)	17.5 years (male)	46,XY	MUD (MC)	Alive 3.5 years

B

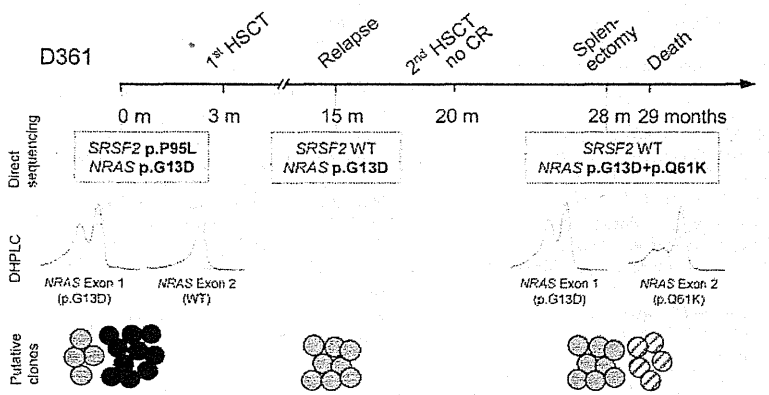

C

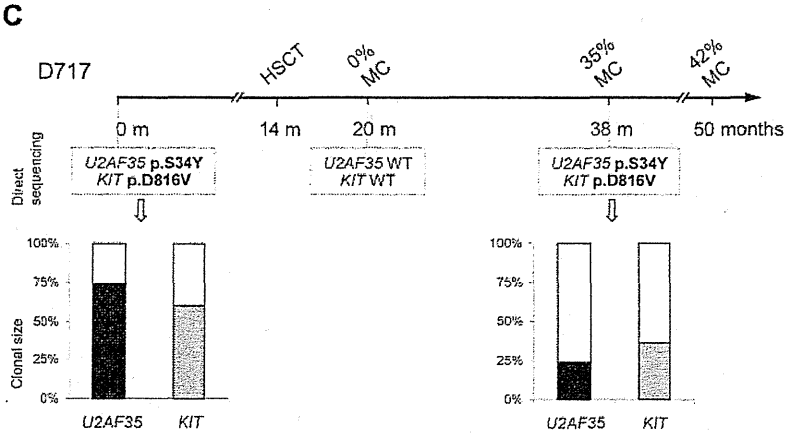

Figure 1. Spliceosome mutations and coexisting oncogenic mutations in children with MDS and JMML. (A) Mutations identified in 3 children. (B) Clinical timeline of patient D361. After second HSCT, the patient did not reach complete remission. Direct sequencing identified an *SRSF2* mutation that was present only at diagnosis but was undetectable at later time points. A mutation in *NRAS* exon 1 (p.G13D) was detectable at all time points. In contrast, the mutation in *NRAS* exon 2 (p.Q61K) was present only at time of disease progression after second HSCT. This was confirmed by denaturing high-performance liquid chromatography. Bold lines represent patients' samples; and dashed lines, a wild-type control DNA. The picture at the bottom illustrates the hypothetical clonal evolution; black circles represent a clone carrying both the *NRAS*(p.G13D) and the *SRSF2* mutation; gray circles, a primary clone harboring only the *NRAS*(p.G13D) mutation; and striped circles, a secondary clone with double *NRAS* mutation (p.G13D and p.Q61K). (C) Clinical timeline of patient D717. Mixed chimerism with 35% autologous cells occurred at 24 months after HSCT. Results from direct sequencing are presented within dashed boxes. The results from allele-specific clonal sequencing are shown at the bottom; the filled bars represent the proportion of mutant *U2AF35* and *KIT* alleles. Twenty-three *U2AF35* and 25 *KIT* subcloned alleles were sequenced in the diagnostic sample, and 25 *U2AF35* and 31 *KIT* subcloned alleles were sequenced in the post-HSCT sample. SM-AHNMD indicates systemic mastocytosis associated with a clonal hematologic nonmast cell lineage disease; RCC, refractory cytopenia of childhood; CR, complete remission; DHPLC, denaturing high-performance liquid chromatography; MRD, matched related donor; MUD, matched unrelated donor; MC, mixed chimerism; and WT, wild-type.

In conclusion, the data reported here suggest that alterations of the spliceosome complex do not constitute a fundamental etiologic factor in pediatric MDS and JMML. First, they are exceedingly rare in a group of diseases that is infrequent in itself. Second, in the positive cases identified here, spliceosome mutations did not occur independently of oncogenic mutations and in 1 case even disappeared during disease evolution. It is reasonable to assume that in children these mutations coexist as passengers in an oncogenic environment alongside primary mutations of signal transduction pathways, known to act as drivers in the malignant process.

Acknowledgments

The authors thank Sandra Urbaniak for excellent technical assistance, Alexandra Fischer and Wilfried Truckenmüller for expert data management, and Annamaria Cseh for case review.

This work was supported by Deutsche Krebshilfe (109005; M.W.W.) and Deutsche Forschungsgemeinschaft (FL345/4-1; C.F.).

Authorship

Contribution: S.H. performed research and analyzed data; C.F. interpreted data and wrote the manuscript; J.M. performed research; M.H., H.H., B.G., T.K., and F.T. recruited patients; B. Schlegelberger reviewed cytogenetics; I.B. reviewed pathology; B. Strahm, J.S., F.L., M.Z., E.B., M.D., M.M.v.d.H.-E., and B.D.M. recruited patients; S.O. designed research; C.M.N. recruited patients and designed research; and M.W.W. designed and performed research and wrote the manuscript.

Conflict-of-interest disclosure: The authors declare no competing financial interests.

Correspondence: Marcin W. Wlodarski, Pediatric Hematology and Oncology, University of Freiburg, Mathildenstr 1, 79106 Freiburg, Germany; e-mail: marcin.wlodarski@uniklinik-freiburg.de.

References

1. Yoshida K, Sanada M, Shiraishi Y, et al. Frequent pathway mutations of splicing machinery in myelodysplasia. *Nature*. 2011;478(7367):64-69.
2. Papaemmanuil E, Cazzola M, Boultwood J, et al. Somatic SF3B1 mutation in myelodysplasia with ring sideroblasts. *N Engl J Med*. 2011;365(15):1384-1395.
3. Visconte V, Makishima H, Jankowska A, et al. SF3B1, a splicing factor is frequently mutated in refractory anemia with ring sideroblasts [published online ahead of print September 2, 2011]. *Leukemia*. doi:10.1038/leu.2011.232.
4. Abdel-Wahab O, Levine R. The spliceosome as an indicted conspirator in myeloid malignancies. *Cancer Cell*. 2011;20(4):420-422.
5. Hofmann WK, Ganser A, Seipelt G, et al. Treatment of patients with low-risk myelodysplastic syndromes using a combination of all-trans retinoic acid, interferon alpha, and granulocyte colony-stimulating factor. *Ann Hematol*. 1999; 78(3):125-130.
6. Stadler M, Germing U, Kliche KO, et al. A prospective, randomised, phase II study of horse antithymocyte globulin vs rabbit antithymocyte globulin as immune-modulating therapy in patients with low-risk myelodysplastic syndromes. *Leukemia*. 2004;18(3):460-465.
7. Passweg JR, Giagounidis AAN, Simcock M, et al. Immunosuppressive therapy for patients with myelodysplastic syndrome: a prospective randomized multicenter phase III trial comparing antithymocyte globulin plus cyclosporine with best supportive care-SAKK 33/99. *J Clin Oncol*. 2011; 29(3):303-309.
8. Porter J. Oral iron chelators: prospects for future development. *Eur J Haematol*. 1989;43(4):271-285.
9. Wlodarski MW, O'Keefe C, Howe EC, et al. Pathologic clonal cytotoxic T-cell responses: nonrandom nature of the T-cell-receptor restriction in large granular lymphocyte leukemia. *Blood*. 2005; 106(8):2769-2780.
10. Baumann I, Niemeyer CM, Bennett JM, Shannon K. Childhood myelodysplastic syndrome. In: *WHO Classification of Tumours of Haematopoietic and Lymphoid Tissues*. Lyon, France: IARC Press; 2008:104-107.
11. Hasle H, Niemeyer CM, Chessells JM, et al. A pediatric approach to the WHO classification of myelodysplastic and myeloproliferative diseases. *Leukemia*. 2003;17(2):277-282.
12. Hasle H, Niemeyer CM. Advances in the prognostication and management of advanced MDS in children. *Br J Haematol*. 2011;154(2):185-195.
13. Vardiman JW, Thiele J, Arber DA, et al. The 2008 revision of the World Health Organization (WHO) classification of myeloid neoplasms and acute leukemia: rationale and important changes. *Blood*. 2009;114(5):937-951.
14. McClintock-Treep SA, Horny HP, Sotlar K, Foucar MK, Reichard KK. KIT(D816V+) systemic mastocytosis associated with KIT(D816V+) acute erythroid leukaemia: first case report with molecular evidence for same progenitor cell derivation. *J Clin Pathol*. 2009; 62(12):1147-1149.
15. Ustun C, Corless CL, Savage N, et al. Chemotherapy and dasatinib induce long-term hematologic and molecular remission in systemic mastocytosis with acute myeloid leukemia with KIT D816V. *Leuk Res*. 2009;33(5):735-741.
16. Wlodarski MW, Motter J, Gorr TA, et al. Abnormal promoter DNA methylation in juvenile myelomonocytic leukemia is not caused by mutation in DNMT3A. *Blood*. 2011;118(16):4490-4491.
17. Muramatsu H, Makishima H, Jankowska AM, et al. Mutations of an E3 ubiquitin ligase c-Cbl but not TET2 mutations are pathogenic in juvenile myelomonocytic leukemia. *Blood*. 2010;115(10): 1969-1975.
18. Sugimoto Y, Muramatsu H, Makishima H, et al. Spectrum of molecular defects in juvenile myelomonocytic leukaemia includes ASXL1 mutations. *Br J Haematol*. 2010;150(1):83-87.
19. Damm F, Thol F, Hollink I, et al. Prevalence and prognostic value of IDH1 and IDH2 mutations in childhood AML: a study of the AML-BFM and DCOG study groups. *Leukemia*. 2011;25(11): 1704-1710.

Specific mitochondrial DNA mutation in mice regulates diabetes and lymphoma development

Osamu Hashizume[a], Akinori Shimizu[a], Mutsumi Yokota[a], Atsuko Sugiyama[a], Kazuto Nakada[a], Hiroyuki Miyoshi[b], Makiko Itami[c], Miki Ohira[d], Hiroki Nagase[e], Keizo Takenaga[f], and Jun-Ichi Hayashi[a,1]

[a]Faculty of Life and Environmental Sciences, University of Tsukuba, Tsukuba, Ibaraki 305-8572, Japan; [b]Subteam for Manipulation of Cell Fate, RIKEN BioResource Center, Tsukuba, Ibaraki 305-0074, Japan; [c]Department of Pathology, Chiba Cancer Center, Chuo-Ku, Chiba 260-8717 Japan; [d]Divisions of Cancer Genomics and [e]Cancer Genetics, Chiba Cancer Center Research Institute, Chuo-Ku, Chiba 260-8717 Japan; and [f]Department of Life Science, Faculty of Medicine, Shimane University, Izumo, Shimane 693-8501, Japan

Edited by Tak W. Mak, The Campbell Family Institute for Breast Cancer Research, Ontario Cancer Institute at Princess Margaret Hospital, University Health Network, Toronto, Canada, and approved May 16, 2012 (received for review February 13, 2012)

It has been hypothesized that respiration defects caused by accumulation of pathogenic mitochondrial DNA (mtDNA) mutations and the resultant overproduction of reactive oxygen species (ROS) or lactates are responsible for aging and age-associated disorders, including diabetes and tumor development. However, there is no direct evidence to prove the involvement of mtDNA mutations in these processes, because it is difficult to exclude the possible involvement of nuclear DNA mutations. Our previous studies resolved this issue by using an mtDNA exchange technology and showed that a G13997A mtDNA mutation found in mouse tumor cells induces metastasis via ROS overproduction. Here, using transmitochondrial mice (mito-mice), which we had generated previously by introducing G13997A mtDNA from mouse tumor cells into mouse embryonic stem cells, we provide convincing evidence supporting part of the abovementioned hypothesis by showing that G13997A mtDNA regulates diabetes development, lymphoma formation, and metastasis—but not aging—in this model.

reactive oxygen species generating mutation | Warburg effect | chromosome aberration | lactic acidosis | hyperglycemia

Pathogenic mitochondrial DNA (mtDNA) mutations that induce significant mitochondrial respiration defects are responsible for mitochondrial diseases (1, 2) and could also be involved in aging and age-associated disorders, including tumor development (1–5). On the other hand, mitochondrial respiration defects caused by nuclear DNA mutations and the resultant enhanced glycolysis under normoxic conditions, i.e., the Warburg effect, are proposed to be involved in tumor development (6–9). Because pathogenic mtDNA mutations also induce mitochondrial respiration defects and up-regulation of aerobic glycolysis, accumulation of these mtDNA mutations with age could also be responsible for tumor development. In addition, it is possible that mtDNA mutations regulate tumor development as a consequence of overproduction of reactive oxygen species (ROS) and the resultant induction of genetic instability (1, 2, 10). In fact, somatic mtDNA mutations are preferentially accumulated in human tumor cells (11–13), and a germline mtDNA mutation (A8344G) in the $tRNA^{L\text{-}ys}$ gene has been found in lipomas (benign adipose tissue tumors) (14). However, there is as yet no direct evidence for the contribution of mtDNA mutations to aging and tumor development, because of the difficulty of excluding the possible contribution of nuclear DNA mutations, including copy-number variants (CNVs), to these processes (2, 15).

Our previous study (16) resolved this issue by using complete mtDNA exchange technology between mouse normal and tumor cells, and we showed that exogenously introduced mtDNA does not affect tumorigenicity. In contrast, our recent study (17) performed exchange of mtDNA between poorly and highly metastatic mouse tumor cells, providing convincing evidence that the somatic mtDNA mutation G13997A in the ND6 gene, which encodes one of the subunits of respiration complex I (NADH dehydrogenase), reversibly controls the development of highly metastatic potential in tumor cells. Moreover, the induction of metastasis is due to overproduction of ROS (17) but not to overproduction of lactates (18). However, these studies have not answered the questions of whether the mutated mtDNA actually controls metastatic phenotypes in living mice and whether it also controls aging and age-associated disorders, including tumor development. Because it is not possible to examine these questions as far as the mutated mtDNA is confined in tumor cells, we performed intercellular transfer of G13997A mtDNA from highly metastatic tumor cells into mouse embryonic stem cells and generated transmitochondrial mito-mice possessing only G13997A mtDNA (19).

This study used aged inbred C57BL/6J (B6) mice and age-matched mito-mice (named mito-miceND6^{M}), which carry G13997A mtDNA but share the B6 nuclear background to exclude the possible involvement of nuclear DNA variations in the phenotypes exclusively developed in aged mito-miceND6^{M}. We examined whether aged mito-miceND6^{M} with G13997A mtDNA introduced from the highly metastatic tumor cells would be susceptible to aging and to age-associated disorders such as tumor development.

Results

Mitochondrial Disease Phenotypes in Aged Mito-MiceND6^{M}. Using the aged transmitochondrial mito-miceND6^{M}, we first examined whether aging enhances respiration defects and the phenotypes associated with mitochondrial diseases. Complex I activity in the tissues of aged mito-miceND6^{M} (18-mo-old males) was about 35–40% lower than that in age-matched B6 males (Fig. 1*A*). In aged mito-miceND6^{M}, ROS were overproduced in bone marrow cells but not in splenocytes (Fig. 1*B*). Considering that young mito-miceND6^{M} (3-mo-old males) show a 30% reduction in complex I activity and no ROS overproduction (19), aging enhanced these phenotypes.

Our previous study (19) also showed that young mito-miceND6^{M} (3-mo-old males) have slight lactic acidosis, a common phenotype in humans with mitochondrial diseases (1, 2) and in mito-mice with other pathogenic mtDNA mutations (20–22). Using aged mito-miceND6^{M} (21-mo-old males), this study reexamined blood lactate levels. We also used mito-miceCOI^{M}, which we had generated previously (21), as positive controls with lactic acidosis due to respiration complex IV defects caused by a pathogenic T6589C mtDNA mutation in the COI gene. Unlike B6 mice, both aged mito-miceND6^{M} and age-matched mito-miceCOI^{M} (21-mo-old males) had slight lactic acidosis in the peripheral blood (Fig. 1*C*). Induction of lactic acidosis, i.e., the Warburg effect, was therefore

Author contributions: O.H. and J.-I.H. designed research; O.H., A. Shimizu, M.Y., A. Sugiyama, and M.O. performed research; O.H., A. Shimizu, K.N., H.M., M.I., H.N., K.T., and J.-I.H. analyzed data; and J.-I.H. wrote the paper.

The authors declare no conflict of interest.

This article is a PNAS Direct Submission.

[1]To whom correspondence should be addressed. E-mail: jih45@biol.tsukuba.ac.jp.

This article contains supporting information online at www.pnas.org/lookup/suppl/doi:10.1073/pnas.1202367109/-/DCSupplemental.

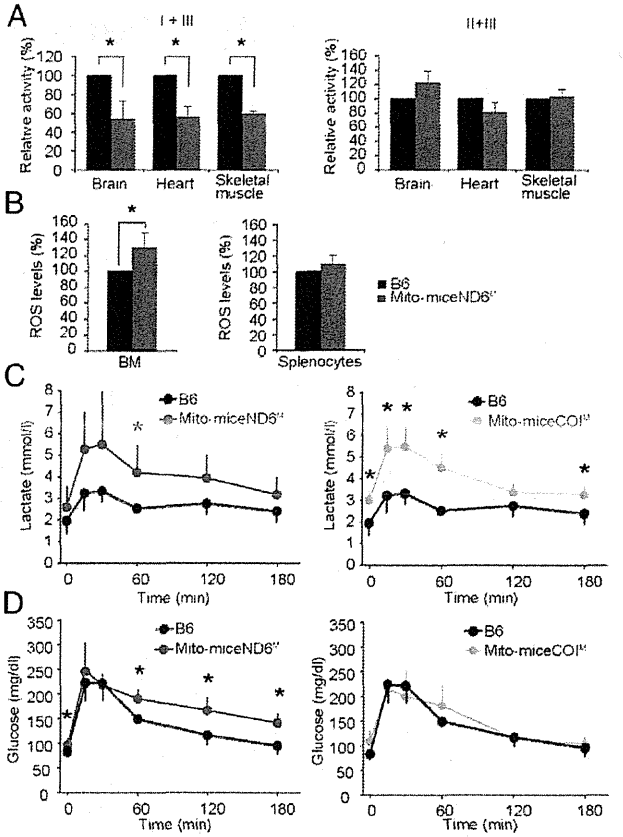

Fig. 1. Examination of the phenotypes associated with mitochondrial diseases in aged mito-miceND6^M. (*A*) Biochemical analysis of mitochondrial respiratory complex activity in the brain, heart, and skeletal muscles. Respiratory complex I (NADH dehydrogenase), complex II (succinate dehydrogenase), and complex III (cytochrome *c* reductase) are components of the electron-transport chain located in the mitochondrial inner membrane. Because the activity of complexes II + III is normal in the tissues of mito-miceND6^M, the reduced activity of complexes I + III observed in mito-miceND6^M should represent complex I defects. Data are represented as mean values with SD (n = 3). *P < 0.05 compared with control B6 mice. (*B*) Estimation of mitochondrial superoxide (i.e., reactive oxygen species, ROS) levels in bone marrow cells and splenocytes after treatment with MitoSOX-Red (Invitrogen). Relative mitochondrial superoxide levels were expressed as mean fluorescence intensity. Data are represented as mean values with SD (n = 3). *P < 0.05 compared with control B6 mice. (*C*) Estimation of blood lactate levels in aged mito-miceND6^M, age-matched B6 mice, and age-matched mito-miceCOI^M before and after glucose administration. Data are represented as mean values with SD (n = 5). *P < 0.05 compared with control B6 mice. (*D*) Estimation of blood glucose levels in aged mito-miceND6^M, age-matched B6 mice, and age-matched mito-miceCOI^M before and after glucose administration. Data are represented as mean values with SD (n = 5). *P < 0.05 compared with control B6 mice.

common to the two mutants (mito-miceND6^M and mito-miceCOI^M), irrespective of whether they were young or aged or whether they express respiration defects in complex I or IV activity.

In addition to lactic acidosis, aged patients with mitochondrial diseases sometimes express diabetes, which is one of the age-associated disorders considered to be caused by mtDNA mutations (1, 2). We therefore examined blood glucose and insulin levels. Although we found no significant differences in blood insulin levels between aged mito-miceND6^M (21-mo-old males) and age-matched B6 males (Fig. S1), aged mito-miceND6^M had higher blood glucose levels after glucose stimulation than did age-matched B6 mice; however, glucose levels in aged mito-miceCOI^M did not differ from those in age-matched B6 mice (Fig. 1*D*). Therefore, all pathogenic mtDNA mutations, inducing mitochondrial respiration defects, do not necessarily cause mitochondrial diabetes. Because the G13997A mutation, but not the T6589C mutation, induces ROS overproduction (17), the increased glucose levels observed exclusively in aged mito-miceND6^M might have resulted not from lactate overproduction but from ROS overproduction. This idea was supported by the results of administration of *N*-acetylcysteine (NAC), an antioxidant, to the mito-miceND6^M: NAC treatment for 1 wk suppressed the glucose intolerance (Fig. S2).

Lifespan and Tumor Formation Frequency in Mito-MiceND6^M. Respiration defects caused by mtDNA mutations and the resultant overproduction of ROS and lactates are also considered to induce aging and age-associated disorders, including tumor formation (1–4, 6–13, 23, 24). We therefore examined this hypothesis by using 35 mito-miceND6^M males and 35 B6 males. We also examined 18 mito-miceCOI^M males as controls expressing lactic acidosis (Fig. 1*C*) to test whether the lactic acidosis common to mito-miceND6^M and mito-miceCOI^M would affect lifespan and tumor formation frequency.

Median survival times of mito-miceND6^M, B6 mice, and mito-miceCOI^M were 24.6, 26.1, and 26.6 mo, respectively. Although mito-miceND6^M had slightly shorter survival times than B6 mice, the difference was not significant (Fig. 2*A*). No leukemic cells were present in the peripheral blood throughout the lifespans of B6 and mutant mice. However, gross necropsy of all dead or euthanized moribund mice showed that 16 of 35 mito-miceND6^M (45.7%) had macroscopic tumor-like abnormalities, including enlarged spleen and liver and lymph node tumors (Table 1 and Fig. 3*A*); similar abnormalities were observed in only 3 of 35 B6 mice (8.6%) and 1 of 18 mito-miceCOI^M (5.6%). The median survival times of mice without tumor-like abnormalities were 25.3 (mito-miceND6^M), 26.0 (B6 mice), and 26.6 mo (mito-miceCOI^M); these differences were not significant (Fig. 2*B*). The slightly shorter median survival times of mito-miceND6^M compared with those of B6 mice (Fig. 2*A*) were therefore at least partly due to the higher frequency of abnormal-tissue formation in aged mito-miceND6^M than in age-matched B6 mice (Table 1).

Histological analyses of abnormal tissues revealed that all were hematopoietic neoplasms and were positive for the pan-leukocyte marker CD45 (Table 1 and Fig. 3*B*). As no leukemic cells were

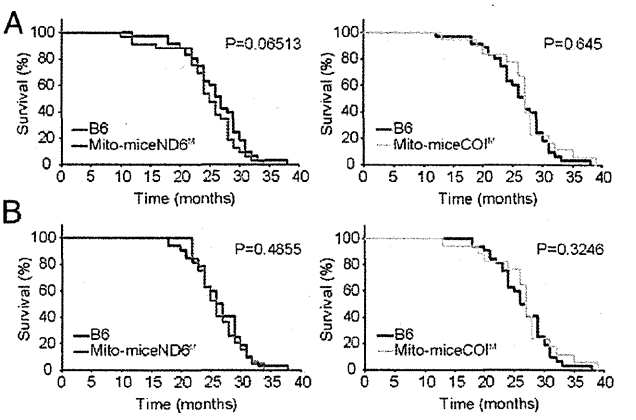

Fig. 2. Kaplan–Meier survival curves of mito-miceND6^M. (*A*) Comparison of lifespan of mice. Median survival times of mito-miceND6^M (n = 35), B6 mice (n = 35), and mito-miceCOI^M (n = 18) were 24.6, 26.1, and 26.6 mo, respectively. Survival curves did not differ significantly. (*B*) Comparison of lifespans of mice that died in the absence of detectable B-cell lymphoma. Median survival times of mito-miceND6^M (n = 19), B6 mice (n = 32), and mito-miceCOI^M (n = 17) were 25.3, 26.0, and 26.6 mo, respectively. Survival curves did not differ significantly.

Table 1. Frequencies of lymphoma in dead or moribund mice

Mouse strain	No. of dead mice	No. of dead mice with tumors (individual code*)	Lifespan, mo	Tissue with tumor				Histological analysis†				Cell type		
				Spleen	Liver	Lung	Lymph node	HE	CD45	B220	CD3	Cell lineage	FL	DLBCL
Mito-mice $ND6^M$	35	16												
		($ND6^M$–31)	29		+		+	Lymphoma	+	+	–	B cell	–	+
		($ND6^M$–29)	28	+				Lymphoma	+	+	–	B cell	–	+
		($ND6^M$–28)	28		+			Lymphoma	+	+	–	B cell	–	+
		($ND6^M$–27)	28	+	+			Lymphoma	+	+	–	B cell	+	–
		($ND6^M$–23)	28	+	+			Lymphoma	+	+	–	B cell	–	+
		($ND6^M$–20)	25		+			Lymphoma	+	+	–	B cell	–	+
		($ND6^M$–18)	24	+			+	Lymphoma	+	+	–	B cell	+	–
		($ND6^M$–13)	23	+			+	Lymphoma	+	–	+	T cell	–	–
		($ND6^M$–11)	22	+	+			Lymphoma	+	+	–	B cell	–	+
		($ND6^M$–7)	19	+				Lymphoma	+	+	–	B cell	–	+
		($ND6^M$–6)	18	+	+	+		Lymphoma	+	+	–	B cell	–	+
		($ND6^M$–5)	18			+		Lymphoma	+	+	–	B cell	–	+
		($ND6^M$–4)	16	+	+	+		Lymphoma	+	+	–	B cell	+	–
		($ND6^M$–3)	12	+				Lymphoma	+	+	–	B cell	–	+
		($ND6^M$–2)	12	+	+			Lymphoma	+	+	–	B cell	–	+
		($ND6^M$–1)	10	+	+			Lymphoma	+	+	–	B cell	+	–
B6	35	3												
		(B6–34)	33		+			Lymphoma	+	+	–	B cell	–	+
		(B6–14)	25				+	Lymphoma	+	+	–	B cell	–	+
		(B6–1)	12		+		+	Lymphoma	+	–	+	T cell	–	–
Mito-mice COI^M	18	1												
		(COI^M–11)	27				+	Lymphoma	+	+	–	B cell	–	+

DLBCL, diffuse large B-cell lymphoma; FL, follicular lymphoma.

*Individual codes were allocated in order of death.

†In most cases, the spleen was the primary B-lymphoma site and the liver and lung were involved secondarily by hematogeneous metastasis (spread), because most of the splenic parenchyma was completely replaced by lymphoma cells, whereas there were multiple small foci of perivascular lymphoma cell infiltration in the liver and lung (Fig. 3*B*). In some cases where tumors were present only in the liver or lung, they were not hepatomas or lung carcinomas, but instead were lymphomas that had spread from the spleen or from lymph nodes near the organs, because all stained positively for CD45 and B220 or CD3.

observed in the peripheral blood (Fig. 3*A*), these hematological neoplasms may have consisted of lymphoma cells. Most tumors were of B-cell origin, expressing the B-cell marker B220 (CD45R) (Fig. 3*B*); they were either follicular lymphoma or diffuse large B-cell lymphoma arising in the spleen, liver, or lung (Table 1). One aged mito-mice$ND6^M$ male and one aged B6 male developed T-cell lymphoma, staining positive for the T-cell marker CD3 (Table 1). These data indicated that mito-mice$ND6^M$ were 750% more prone to lymphoma development than B6 mice in a B-cell–specific manner, providing unambiguous evidence supporting the hypothesis that mitochondrial respiration defects are responsible for tumor formation. However, respiration defects and the resultant lactic acidosis alone could not have been responsible for the frequent B-cell lymphoma formation in the mito-mice$ND6^M$, because aged mito-miceCOI^M, which also showed respiration defects and resultant lactic acidosis (Fig. 1*C*), did not have high frequencies of lymphoma formation (Table 1). It is therefore likely that the ROS overproduction in the bone marrow of mito-mice$ND6^M$ (Fig. 1*B*) is crucial for B-cell lymphoma formation. Analysis of the CNVs showed partial gains of chromosomes 3 and 11 in the spleen with B-cell lymphoma from a mito-mouse$ND6^M$ (Fig. S3), suggesting that G13997A mtDNA and the resultant ROS overproduction and chromosome aberration are involved in B-cell lymphoma development.

Metastatic Potential in Mito-Mice$ND6^M$. Mito-mice$ND6^M$ did not form tumors other than lymphomas during their lifespans (Table 1). Thus, the tumor-inducing effect of G13997A mtDNA might be restricted to lymphoma formation, and it might therefore be difficult to examine the effects of G13997 mtDNA on metastatic potential in mito-mice$ND6^M$. We examined these possibilities by isolating mouse embryonic fibroblasts (MEFs) and testing whether G13997A mtDNA affected their tumor-related phenotypes, such as immortalization of MEFs to lose their finite lifespan, transformation of immortalized MEFs to acquire tumorigenicity, or malignant progression of the transformed MEFs to express metastasis.

We obtained three MEF lines (MEFB6-I, -II, and -III) from three B6 embryos and four lines (MEF$ND6^M$-I, -II, -III, and -IV) from four mito-mice$ND6^M$ embryos (Table S1). By culturing these seven MEF lines using the 3T3 protocol (refs. 25, 26 and *Materials and Methods*), we isolated six immortalized 3T3 lines (3T3B6-I, -II, and -III; 3T3$ND6^M$-I, -II, and -III); we failed to obtain one 3T3 line from a MEF line (MEF$ND6^M$-IV) with G13997A mtDNA (Table S1). The average numbers of cell divisions for the MEF lines to lose their finite lifespan were 7.9 for MEFB6 and 11.0 for MEF$ND6^M$ (Fig. 4*A*), suggesting that at least three additional cell divisions were required for immortality in MEF$ND6^M$ with G13997A mtDNA. Therefore, G13997A mtDNA does not enhance, but instead slightly suppresses, immortalization in MEFs.

Next, we examined the frequency of spontaneous transformation of immortalized 3T3 lines into tumor cells expressing tumorigenicity. After we had established six immortal 3T3 lines, we cultured them for 1 mo to obtain sufficient numbers of cells for inoculation to test their tumorigenicity. After inoculating the cells s.c. into the backs of B6 mice, we observed growing tumor masses only from the inoculation of two 3T3 lines, 3T3B6-III and 3T3$ND6^M$-I, carrying B6 mtDNA and G13997A mtDNA, respectively; the other four 3T3 lines did not form tumor masses (Fig. 4*B*). These four nontransformed 3T3 lines were cultured for 3 mo more to allow spontaneous transformation. They were then inoculated again s.c. into the backs of B6 mice. Two 3T3 lines, 3T3B6-II and 3T3$ND6^M$-III, formed tumors (Fig. 4*B*), probably

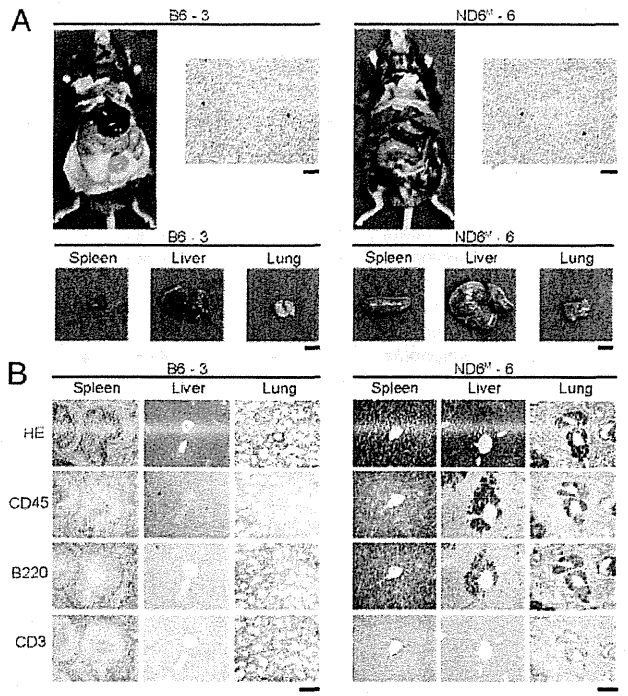

Fig. 3. B-cell lymphoma formation in the tissues of aged mito-miceND6^{M}. (*A*) Gross necropsy of euthanized moribund mice, smear samples of peripheral blood stained by Giemsa, and tissues. *Left* and *Right* panels represent a euthanized moribund B6 mouse without tumors (B6-3) and a euthanized moribund mito-mouseND6^{M} with tumors (ND6^{M}-6), respectively. (Scale bars, 1 cm.) Giemsa-stained preparations show the absence of leukemic cells in the peripheral blood of both B6-3 and ND6^{M}-6. (Scale bars, 50 μm.) (*B*) Histological analyses of serial sections of the tissues to identify B-cell lymphoma. HE, hematoxylin and eosin staining to show tumor formation; CD45, immunohistochemistry using antibody to CD45 to detect leukocytes; B220, immunohistochemistry using antibody to B220 to detect B cells; CD3, immunohistochemistry using antibody to CD3 to detect T cells. Whereas the tissues of B6-3 have a normal structure (*Left*), those of ND6^{M}-6 show abnormal growth of B-lymphoma cells, because they were stained positively with CD45 and B220, but not with CD3 (*Right*). The spleen was the primary B-lymphoma site, whereas the liver and lung were secondarily involved through hematogenous metastasis: most of the splenic parenchyma was completely replaced by lymphoma cells, whereas there were multiple small foci of perivascular lymphoma cell infiltration in the liver and lung. (Scale bars, 200 μm.)

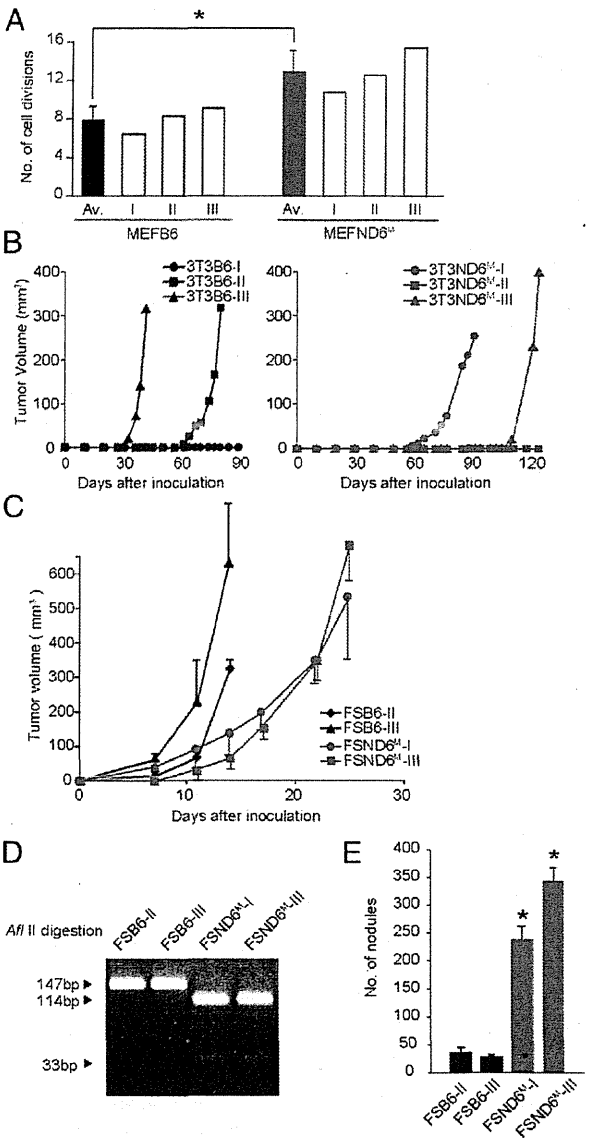

Fig. 4. Characterization of mouse embryonic fibroblasts (MEFs) and MEF-derived cell lines isolated from mito-miceND6^{M}. (*A*) Numbers of cell divisions of MEF lines required for immortalization. Av, average number of cell divisions. Data are represented as mean values with SD ($n = 3$). *$P < 0.05$ compared with control B6 mice. (*B*) Transformation frequencies of immortalized MEF (3T3) lines to express tumorigenicity. (*C*) Tumor growth of the transformed 3T3 (fibrosarcoma) lines isolated from tumor masses formed (Fig. 4*B*). Data are represented as mean values with SD ($n = 3$). (*D*) Identification of mtDNA genotypes of transformed 3T3 (fibrosarcoma) lines. The G13997A mtDNA in FSND6^{M}-I and -III produced 114- and 33-bp fragments owing to the gain of an AflII site by the G13997A substitution in the *ND6* gene, whereas B6 mtDNA without the mutation in FSB6-II and -III produced uncut 147-bp fragments. (*E*) Metastatic potentials of the transformed 3T3 lines (i.e., fibrosarcoma lines). Data are represented as mean values with SD ($n = 3$). *$P < 0.05$ compared with two B6 fibrosarcoma lines.

because of their spontaneous transformation to acquire tumorigenicity during prolonged cultivation. These observations suggest that some of the cells in the populations of the four immortal 3T3 lines had already been transformed spontaneously, and that G13997A mtDNA did not necessarily enhance the transformation frequency of immortalized 3T3 cells to acquire tumorigenicity.

To purify the transformed cells in the population of the four 3T3 line, tumor masses formed from the inoculations under the skin of B6 mice (Fig. 4*B*) were cut into small pieces and placed back into culture medium. Growing cells in culture were obtained from all tumor masses. These cells were then inoculated again s.c. into the backs of B6 mice. All of them rapidly formed tumor masses (Fig. 4*C*), suggesting that they were fibrosarcoma lines expressing tumorigenicity. The lines were named FSB6-II, FSB6-III, FSND6^{M}-I, and FSND6^{M}-III (Table S1). FSB6-II and FSB6-III were confirmed to possess wild-type (B6) mtDNA, and FSND6^{M}-I and FSND6^{M}-III possessed G13997A mtDNA (Fig. 4*D*).

We then examined the metastatic potential of the fibrosarcoma lines by inoculating them i.v. into B6 mice and counting nodule numbers in the lung. This malignant tumor phenotype was exclusively enhanced in the fibrosarcoma cell lines FSND6^{M}-I and -III (Fig. 4*E*), which carried G13997A mtDNA (Fig. 4*D*), even though their primary tumor growth was slower than that of FSB6-II and -III (Fig. 4*C*), which had B6 mtDNA (Fig. 4*D*). Therefore, G13997A mtDNA did not enhance immortalization and transformation of MEFs, but it enhanced the malignant progression of spontaneously transformed MEFs to acquire high metastatic potential.

Discussion

Here, we used aged mito-miceND6^M with pathogenic G13997A mtDNA to examine conventional mitochondrial theory (1–5) proposing that respiration defects caused by pathogenic mtDNA mutations and the resultant ROS or lactate overproduction are responsible for aging and age-associated disorders. As controls, we used age-matched B6 mice with normal mtDNA and mito-miceCOI^M mice with pathogenic T6589C mtDNA (21), which induces respiration defects and the resultant lactate overproduction but not ROS overproduction (17). All of the mice used in this study shared the B6 nuclear DNA background, thus excluding the possible involvement of nuclear genetic variations in the phenotypes exclusively developed in mito-miceND6^M. The results showed that neither G13997A mtDNA nor T6589C mtDNA enhanced aging, but that G13997A mtDNA induced B-lymphoma formation and glucose intolerance, whereas T6589C mtDNA did not. Therefore, this study provides convincing evidence that some pathogenic mtDNA mutations, such as the G13997A mutation, regulate age-associated disorders, including B-lymphoma development and diabetes, in living mice. Moreover, G13997A mtDNA appeared to play various roles in the multiple steps required for MEF transformation. For example, G13997A mtDNA slightly suppressed immortalization of MEFs to lose their finite lifespan (Fig. 4*A*), and it did not induce transformation of immortalized MEFs to acquire tumorigenicity (Fig. 4*B*). However, it did induce malignant progression of the transformed MEFs to express high metastatic potential (Fig. 4*E*). These results are consistent with our previous observations (17): using an in vitro culture system we previously showed that the G13997A mutation induced malignant progression of lung carcinoma cells to acquire high metastatic potential, but it did not induce transformation of immortalized National Institutes of Health 3T3 cells to acquire tumorigenicity (17). Therefore, our finding here that the mutation induced frequent B-lymphoma development in mito-miceND6^M (Table 1) was unexpected.

The question that then arises is why there were only hematological malignancies (Table 1) despite the fact that respiration defects affected all of the tissues examined (Fig. 1*A*). One answer to this tissue-specific tumor development is that the nuclear genetic background of the B6 mice used in this study made them prone to B-lymphoma formation but not to other tumors during their lifespans (Table 1). This idea can be examined by generating mito-miceND6^M carrying G13997A mtDNA but in a nuclear genetic background derived from another wild-type mouse strain that preferentially develops tumors other than B lymphoma. It has been proposed that nuclear genetic variations among wild-type mouse strains affect the tumor formation spectrum (27–30), particularly when genetic manipulations are performed to induce tumor development (29, 30). Thus, the generation of new mito-miceND6^M would be effective for examining the issue of whether G13997A mtDNA enhances the development of different tumors in different nuclear genetic backgrounds or whether it specifically enhances B-lymphoma development irrespective of whether the nuclear genetic background is derived from B6 or not.

Another question is the nature of the mechanism of B-lymphoma development in mito-miceND6^M. Analysis of CNVs showed partial gains of chromosomes 3 and 11 in a spleen with B lymphoma from a mito-mouseND6^M (Fig. S3). Thus, one possible mechanism could be chromosomal instability caused by G13997A mtDNA-mediated overproduction of ROS. It has been proposed that oxidative stress induces various types of cellular damage, leading to chromosome instability that can result in tumor development (10). Moreover, B lymphomas can be frequently induced as a consequence of chromosome translocation (31). Precise chromosome analysis may therefore reveal the mechanism of frequent B-lymphoma formation in mito-miceND6^M.

With respect to the aging of mito-miceND6^M, the G13997A mutation does not solely enhance aging or regulate premature aging phenotypes, which have been reported in mtDNA mutator mice possessing nuclear-coded mtDNA polymerase with a defective proofreading function and expressing the resultant mitochondrial respiration defects but not ROS overproduction (32–34). Absence of the premature aging phenotypes in mito-miceND6^M is not unexpected, because there is no evidence that patients with mitochondrial diseases due to pathogenic mtDNA mutations develop generalized premature aging. Therefore, the introduction of different nuclear genetic backgrounds or nuclear DNA variations into mito-miceND6^M may be required to trigger the onset of their premature aging phenotypes.

Our results also suggested that the glucose intolerance observed exclusively in aged mito-miceND6^M (Fig. 1*D*) resulted from ROS overproduction. This idea was confirmed by the observation that NAC administration suppressed glucose intolerance (Fig. S2). Continuous NAC administration could therefore be an effective therapy for improving ROS-mediated diabetic phenotypes. Because it has been proposed that ROS negatively controls insulin secretion from pancreatic β cells or glucose incorporation into insulin-targeted organs in humans (35), mito-miceND6^M would be effective models for precise investigation of the mechanisms of ROS-mediated diabetes. On the other hand, a reduction in ATP content caused by mitochondrial respiration defects in pancreatic β cells has also been proposed to suppress their insulin secretion and could thus be responsible for inducing mitochondrial diabetes (36). In fact, patients with mitochondrial diseases who carry an A3243G mtDNA mutation in the mitochondrial tRNA$^{Leu(UUR)}$ gene frequently express diabetic phenotypes (1, 35, 37). However, other pathogenic mtDNA mutations are not necessarily correlated with these phenotypes (37). Our mito-miceCOI^M did not show glucose intolerance (Fig. 1*D*), indicating that respiration defects do not always induce diabetic phenotypes. Other mito-mice carrying a pathogenic mutation in the mitochondrial tRNA$^{Leu(UUR)}$ gene will therefore have to be generated to resolve this controversy over the pathogenesis of mitochondrial diabetes.

Materials and Methods

Mice. Inbred B6 mice generated by sibling mating more than 40 times were obtained from CLEA Japan. Mito-miceND6^M (19) and mito-miceCOI^M (21) were generated in our previous works. We maintained B6 mice, mito-miceND6^M, and mito-miceCOI^M sharing a common nuclear DNA background by repeated backcrossing of their females with B6 males. Animal experiments were performed in accordance with protocols approved by the experimental animal committee of the University of Tsukuba, Japan.

Cell Lines and Cell Culture. The mouse cell lines obtained were grown in DMEM (Sigma) containing 10% (vol/vol) FCS, uridine (50 ng/mL), and pyruvate (0.1 mg/mL).

Biochemical Measurement of Respiratory Enzyme Activity. Mitochondrial respiratory complex I (NADH dehydrogenase), complex II (succinate dehydrogenase), and complex III (cytochrome *c* reductase) are components of the electron-transport chain and are located in the mitochondrial inner membrane. The activity of these enzymes was assayed as described previously (11). Briefly, to estimate complex I + III activity, NADH and cytochrome *c* (oxidized form) were used as substrates and the reduction of cytochrome *c* was monitored by measuring absorbance at a wavelength of 550 nm. To estimate complex II + III activity, sodium succinate and cytochrome *c* (oxidized form) were used as substrates, and the reduction of cytochrome *c* was monitored as described above.

Measurement of ROS Production in Mitochondria. ROS generation was detected with the mitochondrial superoxide indicator MitoSOX-Red (Invitrogen). Cells were incubated with 1 mM MitoSOX-Red for 15 min at 37 °C in PBS, washed twice with PBS, and then immediately analyzed with a FACScan flow cytometer (Becton Dickinson).

Lactate and Glucose Measurement. To determine fasting blood lactate and glucose concentrations, blood was collected from the tail veins of mice after overnight starvation. After oral administration of glucose (1.5 g/kg body

weight), blood was again collected, and lactate and glucose concentrations were measured with an automatic blood lactate test meter (Lactate Pro; Arkray) and glucose test meter (Dexter ZII; Bayer), respectively.

Blood Insulin Measurement. Peripheral blood was collected from tail veins. After centrifugation of the blood at 1,000 × g for 15 min at 4 °C, the plasma fraction collected from the supernatant was used to estimate blood insulin levels with a mouse insulin ELISA kit (Shibayagi).

Histological Analyses. Formalin-fixed, paraffin-embedded serial sections were used for histological analyses. Hematoxylin-and-eosin–stained sections were used for histopathological analysis to identify tumor tissues. The immunohistochemical analysis was performed with antibody to CD45 (BD Biosciences) to determine whether the tumor tissues originated from leukocytes, and subsequently with antibodies to B220 (BD Biosciences) and CD3 (Santa Cruz) to determine whether the tumor tissues were of B-cell or T-cell origin, respectively.

Analysis of CNVs. Copy-number variations in nuclear DNA were examined by comparative genomic hybridization array (CGH) using a 4 × 44 k whole-genome array (Agilent Technologies; G4426B#15028). DNA (1 μg) derived from each male mouse spleen was used. A dye-swap experiment was conducted to confirm the results. The protocol for DNA digestion, labeling, purification, and hybridization to the arrays followed the manufacturer's instructions (Agilent Technologies).

Isolation of Immortal 3T3 Cells from MEFs. MEFs in a 6-cm culture dish at a density of 3×10^5 cells per dish were cultured by using the 3T3 protocol reported previously (25, 26). Briefly, 3 d after the cells had been plated at 3×10^5 cells per dish, we trypsinized them, counted the total cell numbers, and then replated 3×10^5 cells into 6-cm dishes. These processes were repeated until immortalized cells appeared.

Genotyping of mtDNAs. Total cellular DNA (0.2 mg) extracted from cultured cells was used as a template. To detect the G13997A mutation, a 147-bp fragment containing the 13,997 site was amplified by using PCR. The nucleotide sequences from nucleotide positions 13,963–13,996 (5′-CCCACTAACAATTAA-ACCTAAACCTCCATActTA-3′; small letters indicate the mismatch site) and nucleotide positions 14,109–14,076 (5′-TTCATGTCATTGGTCGCAGTTGAATGCTG-TGTAG-3′) were used as oligonucleotide primers. Combination of the PCR-generated mutation with the G13997A mutation created a restriction site for AflII and generated 114-bp and 33-bp fragments on AflII digestion. Restriction fragments were separated by electrophoresis on 3% agarose gels containing ethidium bromide (0.1 mg/mL).

Assays of Metastatic Potential and Tumorigenicity. To test for experimental metastatic potential, cells (5×10^5/100 μL PBS) were injected into the tail vein of 6-wk-old male B6 mice (CLEA Japan). The mice were euthanized 23 d later, and their lungs were removed. The lungs were fixed in Bouin's solution and parietal nodules were counted. To assess tumorigenicity, growing cells (5×10^6 cells) suspended in 100 μL PBS were injected s.c. into the backs of 5 wk-old male B6 mice. Tumor growth was monitored assuming spherical growth. When a tumor mass was detectable visually, its maximum (*a*) and minimum (*b*) diameters and height (*h*) were recorded twice a week. The volume of each tumor (*V*) was calculated according to the formula $V = \pi abh/6$.

Statistical Analysis. We analyzed data with the (unpaired or paired) Student *t* test. Kaplan–Meier curves were assessed with the log-rank test. Values with $P < 0.05$ were considered significant.

ACKNOWLEDGMENTS. This work was supported by Grants-in-Aid for Scientific Research S 19100007 (to J.-I.H.), Scientific Research A 23240058 (to K.N.), and Scientific Research on Innovative Areas 24117503 (to J.-I.H.) from Japan Society for the Promotion of Science.

1. Wallace DC (1999) Mitochondrial diseases in man and mouse. *Science* 283:1482–1488.
2. Taylor RW, Turnbull DM (2005) Mitochondrial DNA mutations in human disease. *Nat Rev Genet* 6:389–402.
3. Jacobs HT (2003) The mitochondrial theory of aging: Dead or alive? *Aging Cell* 2: 11–17.
4. Khrapko K, Vijg J (2009) Mitochondrial DNA mutations and aging: Devils in the details? *Trends Genet* 25:91–98.
5. Loeb LA, Wallace DC, Martin GM (2005) The mitochondrial theory of aging and its relationship to reactive oxygen species damage and somatic mtDNA mutations. *Proc Natl Acad Sci USA* 102:18769–18770.
6. Baysal BE, et al. (2000) Mutations in SDHD, a mitochondrial complex II gene, in hereditary paraganglioma. *Science* 287:848–851.
7. Niemann S, Müller U (2000) Mutations in SDHC cause autosomal dominant paraganglioma, type 3. *Nat Genet* 26:268–270.
8. Gottlieb E, Tomlinson IP (2005) Mitochondrial tumour suppressors: A genetic and biochemical update. *Nat Rev Cancer* 5:857–866.
9. Koppenol WH, Bounds PL, Dang CV (2011) Otto Warburg's contributions to current concepts of cancer metabolism. *Nat Rev Cancer* 11:325–337.
10. Klaunig JE, Kamendulis LM, Hocevar BA (2010) Oxidative stress and oxidative damage in carcinogenesis. *Toxicol Pathol* 38:96–109.
11. Polyak K, et al. (1998) Somatic mutations of the mitochondrial genome in human colorectal tumours. *Nat Genet* 20:291–293.
12. Fliss MS, et al. (2000) Facile detection of mitochondrial DNA mutations in tumors and bodily fluids. *Science* 287:2017–2019.
13. He Y, et al. (2010) Heteroplasmic mitochondrial DNA mutations in normal and tumour cells. *Nature* 464:610–614.
14. Larsson NG, Tulinius MH, Holme E, Oldfors A (1995) Pathogenetic aspects of the A8344G mutation of mitochondrial DNA associated with MERRF syndrome and multiple symmetric lipomas. *Muscle Nerve* 3:S102–S106.
15. Augenlicht LH, Heerdt BG (2001) Mitochondria: Integrators in tumorigenesis? *Nat Genet* 28:104–105.
16. Akimoto M, et al. (2005) Nuclear DNA but not mtDNA controls tumor phenotypes in mouse cells. *Biochem Biophys Res Commun* 327:1028–1035.
17. Ishikawa K, et al. (2008) ROS-generating mitochondrial DNA mutations can regulate tumor cell metastasis. *Science* 320:661–664.
18. Ishikawa K, et al. (2008) Enhanced glycolysis induced by mtDNA mutations does not regulate metastasis. *FEBS Lett* 582:3525–3530.
19. Yokota M, et al. (2010) Generation of trans-mitochondrial mito-mice by the introduction of a pathogenic G13997A mtDNA from highly metastatic lung carcinoma cells. *FEBS Lett* 584:3943–3948.
20. Inoue K, et al. (2000) Generation of mice with mitochondrial dysfunction by introducing mouse mtDNA carrying a deletion into zygotes. *Nat Genet* 26:176–181.
21. Kasahara A, et al. (2006) Generation of trans-mitochondrial mice carrying homoplasmic mtDNAs with a missense mutation in a structural gene using ES cells. *Hum Mol Genet* 15:871–881.
22. Nakada K, et al. (2004) Accumulation of pathogenic DeltamtDNA induced deafness but not diabetic phenotypes in mito-mice. *Biochem Biophys Res Commun* 323: 175–184.
23. Shidara Y, et al. (2005) Positive contribution of pathogenic mutations in the mitochondrial genome to the promotion of cancer by prevention from apoptosis. *Cancer Res* 65:1655–1663.
24. Petros JA, et al. (2005) mtDNA mutations increase tumorigenicity in prostate cancer. *Proc Natl Acad Sci USA* 102:719–724.
25. Todaro GJ, Green H (1963) Quantitative studies of the growth of mouse embryo cells in culture and their development into established lines. *J Cell Biol* 17:299–313.
26. Sun H, Taneja R (2007) Analysis of transformation and tumorigenicity using mouse embryonic fibroblast cells. *Methods Mol Biol* 383:303–310.
27. Krupke DM, Begley DA, Sundberg JP, Bult CJ, Eppig JT (2008) The Mouse Tumor Biology database. *Nat Rev Cancer* 8:459–465.
28. Balmain A, Nagase H (1998) Cancer resistance genes in mice: Models for the study of tumour modifiers. *Trends Genet* 14:139–144.
29. Harvey M, McArthur MJ, Montgomery CA, Jr., Bradley A, Donehower LA (1993) Genetic background alters the spectrum of tumors that develop in p53-deficient mice. *FASEB J* 7:938–943.
30. Freeman D, et al. (2006) Genetic background controls tumor development in PTEN-deficient mice. *Cancer Res* 66:6492–6496.
31. Küppers R (2005) Mechanisms of B-cell lymphoma pathogenesis. *Nat Rev Cancer* 5: 251–262.
32. Trifunovic A, et al. (2004) Premature ageing in mice expressing defective mitochondrial DNA polymerase. *Nature* 429:417–423.
33. Kujoth GC, et al. (2005) Mitochondrial DNA mutations, oxidative stress, and apoptosis in mammalian aging. *Science* 309:481–484.
34. Trifunovic A, et al. (2005) Somatic mtDNA mutations cause aging phenotypes without affecting reactive oxygen species production. *Proc Natl Acad Sci USA* 102:17993–17998.
35. Evans JL, Goldfine ID, Maddux BA, Grodsky GM (2003) Perspectives in diabetes: Are oxidative stress-activated signalling pathways mediators of insulin resistance and beta-cell dysfunction? *Diabetes* 52:1–8.
36. Maechler P, Wollheim CB (2001) Mitochondrial function in normal and diabetic β-cells. *Nature* 414:807–812.
37. Maassen JA, et al. (2004) Mitochondrial diabetes: Molecular mechanisms and clinical presentation. *Diabetes* 53(Suppl 1):S103–S109.